

# The Sunyaev-Zel'dovich Effect: Results and Future Prospects

J. E. Carlstrom<sup>a</sup>, M. Joy<sup>b</sup>, L. Grego<sup>c</sup>, G. Holder<sup>a</sup>,  
W. L. Holzapfel<sup>d</sup>, S. LaRoque<sup>a</sup>, J. J. Mohr<sup>e</sup> and E. D. Reese<sup>a</sup>  
*to appear in "Constructing the Universe with Clusters of Galaxies",  
IAP conference, July 2000, eds. F. Durret and G. Gerbal,  
<http://www.iap.fr/Conferences/Colloque/coll2000/>*

The Sunyaev-Zel'dovich effect (SZE) provides a powerful tool for cosmological studies. Through recent advances in instrumentation and observational techniques it is now possible to obtain high quality measurements of the effect toward galaxy clusters. The analysis of the SZE toward a few tens of clusters has already led to interesting constraints on the Hubble constant and the mass density of the universe. In the near future, instruments exploiting the redshift independence of the SZE will be used to conduct deep surveys for galaxy clusters providing detailed information on the growth of large scale structure, tests of cosmological models and tight constraints on the cosmological parameters that describe our universe. In this review we provide an overview of the SZE and its use for cosmological studies. We summarize the current state of observations and the constraints on cosmological parameters already obtained and we discuss the power of using the SZE for future deep cluster surveys.

## 1 Introduction

The Sunyaev-Zel'dovich Effect (SZE) provides a unique and powerful observational tool for cosmology. It is particularly useful for determining cosmological parameters when combined with other observational diagnostics of clusters of galaxies such as X-ray emission from the intracluster gas, weak and strong lensing by the cluster potential, and optical galaxy velocity dispersion measurements. For example, cluster distances can be determined from the analysis of SZE and X-ray data, leading to an estimate of the Hubble constant and eventually the deceleration parameter. The baryonic and total masses of clusters can be measured directly, allowing an estimate of the ratio of the baryonic to total matter density of the universe.

All of the measurements provide insights into the structure of galaxy clusters themselves. Furthermore, many of the cluster properties derived directly from a given observation, or from a combination of observations, can be determined in several different ways. For example, the gas mass fraction can be determined by various combinations of SZE, X-ray, and lensing observations. The electron temperature, a direct measure of a cluster's mass, can be measured directly through X-ray spectroscopy, or determined through the analysis of various combinations of X-ray, SZE, and lensing observations. Many of the desired properties of clusters are therefore over-constrained by observation, allowing a deeper understanding of clusters and critical tests of current models for the formation and evolution of galaxy clusters.

Perhaps the most unique and powerful cosmological tool provided by the exploitation of the SZE is the possibility to conduct deep large scale surveys for galaxy clusters. SZE observations are particularly well suited for deep surveys because the detection threshold for such a survey depends on the mass of the cluster and is independent of distance. *SZE surveys will be able to detect all clusters above a mass limit independent of the redshift of the clusters.* This remarkable property of SZE surveys is due to the fact that the SZE is a distortion of the CMB spectrum.

---

<sup>a</sup>Dept. of Astronomy and Astrophysics, University of Chicago, 5640 S. Ellis Ave., Chicago, IL 60637

<sup>b</sup>Space Science Laboratory, SD50, NASA Marshall Space Flight Center, Huntsville, AL 35812

<sup>c</sup>Harvard-Smithsonian Center for Astrophysics, 60 Garden Street, Cambridge, MA 02138

<sup>d</sup>Dept. of Physics, University of California, Berkeley, Berkeley, CA 94720

<sup>e</sup>Depts. of Astronomy, Physics, University of Illinois, Urbana, IL 61801

While the CMB suffers cosmological dimming with redshift, the ratio of the SZE to the CMB does not; it is a direct, redshift independent measurement of the intracluster medium (ICM) column density weighted by temperature, i.e., the pressure integrated along the line of sight. The total SZE flux detected will be proportional to the total temperature-weighted mass (total integrated pressure) and inversely proportional to the square of the angular diameter distance. Adopting a reasonable cosmology and accounting for the increase in the universal matter density with redshift, the mass limit for a given SZE survey flux sensitivity will rise with redshift, level off at redshifts approaching one and actually decrease at redshifts greater than one.

There has been considerable progress recently in detecting and imaging the SZE. Efforts over the first two decades after the SZE was first proposed in 1970<sup>1,2</sup> yielded only a couple of reliable detections. Over the last decade new detectors and observing techniques have allowed high quality detections and images of the effect for more than 40 clusters with redshifts as high as 0.9. Now at the start of the fourth decade we are in position to exploit fully the power of the SZE by obtaining detailed images of a set of clusters to understand the ICM, by observing large SZE samples of clusters to determine statistically robust estimates of the cosmological parameters, and to commence large untargeted SZE surveys to probe the high redshift universe. These surveys will provide a direct view of the growth of large scale structure and allow constraints to be placed on the equation of state of the dark energy.<sup>3,4</sup>

In this brief review, we first outline the properties of the SZE and its use for cosmological studies. Next we provide an overview of the current observational techniques with examples of recent results and a summary of observations obtained to date. The constraints that have been placed on cosmological parameters are given next. Finally, we discuss the expectations for future SZE observations and their role in cosmological studies.

## 2 The Sunyaev-Zel'dovich Effect

The Sunyaev-Zel'dovich effect (SZE) is a small spectral distortion of the cosmic microwave background (CMB) caused by the scattering of CMB photons off a distribution of high energy electrons. Here we concentrate on the SZE caused by the hot thermal distribution of electrons provided by the intracluster medium (ICM) of massive galaxy clusters. The average energy exchange in the scattering of a CMB photon off an electron is  $k_B T_e / m_e c^2$ .

The derivation of the SZE can be found in the original papers of Sunyaev and Zel'dovich,<sup>1,2</sup> in several reviews,<sup>6,7,8</sup> and in a number of more recent contributions which include relativistic corrections.<sup>7,9,10,11,12,13</sup>

The SZE distortion of the CMB spectrum at dimensionless frequency  $x \equiv \frac{h\nu}{k_B T_{CMB}}$  is given by

$$\frac{\Delta T_{SZE}}{T_{CMB}} = f(x, T_e) y, \quad (1)$$

where  $y$  is the Compton  $y$ -parameter equal to the optical depth,  $\tau_e = \sigma_T \int n_e dl$ , times the fractional energy gain per scattering

$$y = \sigma_T \int n_e \frac{k_B T_e}{m_e c^2} dl, \quad (2)$$

with  $\sigma_T$  the Thomson cross-section,  $n_e$  the electron number density,  $T_e$  the electron temperature,  $k_B$  the Boltzmann constant,  $m_e c^2$  the electron rest mass energy and the integration is along the line of sight.

The spectral distortion as a function of the dimensionless frequency is given by

$$f(x, T_e) = \left( x \frac{e^x + 1}{e^x - 1} - 4 \right) (1 + \delta_{SZE}(x, T_e)), \quad (3)$$

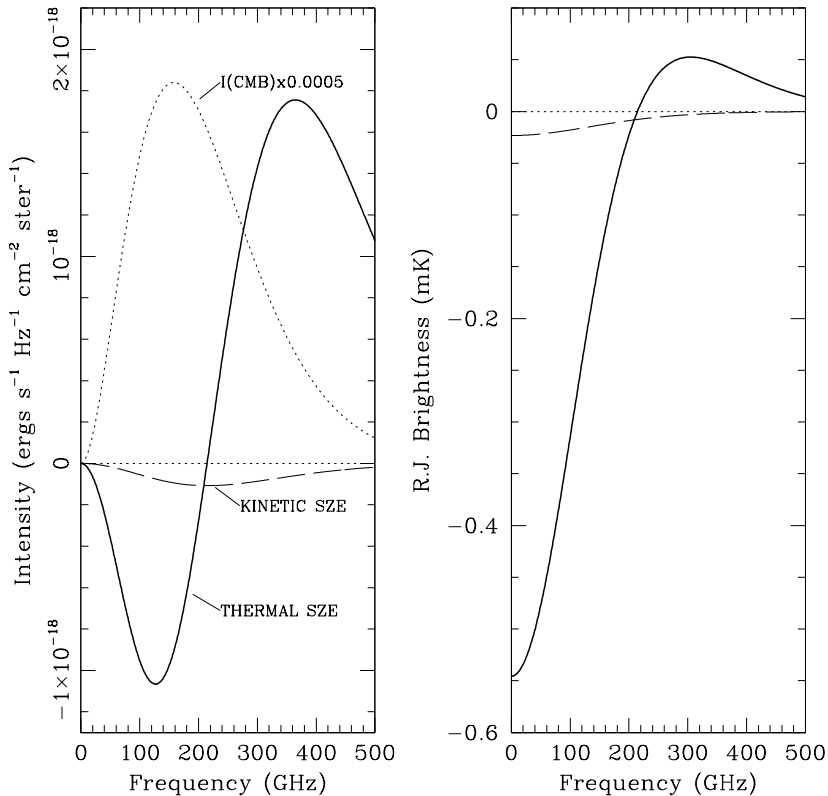


Figure 1: Spectral distortion of the cosmic microwave background (CMB) radiation due to the Sunyaev-Zel'dovich effect (SZE). The left panel shows the intensity and the right panel shows the Rayleigh-Jeans brightness temperature. The thick solid line is the thermal SZE and the dashed line is the kinetic SZE. For reference the 2.728 K Planck spectrum of the CMB<sup>5</sup> (scaled by 0.0005) is shown by the dotted line in the left panel; a line at zero is shown in both panels. The cluster properties used to calculate the spectra are an electron temperature of 10 keV, a Compton  $y$  parameter of  $10^{-4}$  and a peculiar velocity of  $500 \text{ km s}^{-1}$ .

where  $\delta_{SZE}(x, T_e)$  is the relativistic correction to the frequency dependence. Note that  $f(x, T_e) \rightarrow -2$  in the non-relativistic and Rayleigh-Jeans (RJ) limits.

If the cluster is moving with respect to the CMB rest frame with a component of its velocity,  $v_{pec}$ , projected along the line of sight to the cluster, then the observed distortion of the CMB spectrum will have a component due to the Doppler effect referred to as the kinetic SZE. In the non-relativistic limit, the spectral signature of the kinetic SZE is a purely thermal distortion of magnitude

$$\Delta T/T_{CMB} = -\tau_e(v_{pec}/c), \quad (4)$$

where  $v_{pec}$  is along the line of sight; the emergent spectrum is still described completely by a Planck spectrum, but at a slightly different temperature, lower (higher) for positive (negative) peculiar velocities.<sup>2,14,8</sup>

Fig. 1 illustrates the spectral distortions of the CMB induced by the thermal and kinetic SZE of a massive cluster. The left panel shows the change in intensity and the right panel shows the change in Rayleigh-Jeans (RJ) brightness temperature. The RJ brightness is shown because the sensitivity of a radio telescope is calibrated in these units. It is defined simply by  $I_\nu = (2k_B\nu^2/c^2)T_{RJ}$  where  $I_\nu$  is the intensity at frequency  $\nu$ ,  $k_B$  is Boltzmann's constant and  $c$

is the speed of light. The Planck spectrum of the CMB radiation is also shown by the dotted line (multiplied by 0.0005) for reference. Note that the thermal effect causes a decrement at low frequencies ( $\nu < 218$  GHz) and an increment at high frequencies and is distinguished readily from a simple temperature fluctuation of the CMB. The kinetic SZE distortion is shown by the dashed curve. In the non-relativistic regime, it is indistinguishable from a CMB temperature fluctuation.

The gas temperatures measured in massive galaxy clusters are around  $k_B T_e \sim 10$  keV.<sup>15,16</sup> At these temperatures, electron velocities are becoming relativistic and small corrections are required to calculate the proper SZE. For a massive cluster with  $k_B T_e / m_e c^2 \sim 0.02$  the relativistic corrections to the SZE are of order a few percent in the RJ portion of the spectrum, but can be substantial near the null of the thermal effect. Convenient analytical approximations to fifth order in  $k_B T_e / m_e c^2$  are presented in Itoh et al.<sup>10</sup>

Relativistic perturbations to the kinetic SZE are due to the Lorentz boost to the electrons provided by the bulk velocity.<sup>12,13</sup> The leading term is of order  $(k_B T_e / m_e c^2)(v/c)$  and for a 10 keV cluster moving at  $1000 \text{ km s}^{-1}$  the effect is about an 8% correction. The  $(k_B T_e / m_e c^2)^2(v/c)$  term is about 1%, and the  $(v/c)^2$  term is only 0.2%.

### 3 Cosmology with the Sunyaev-Zel'dovich Effect

The unique aspect of using the SZE for cosmology is that it is simply a measure of the column density of electrons weighted by temperature. The total SZE flux of a cluster is also a clean measure of the total energy of the cluster.

The SZE is perhaps best known for enabling an independent determination of the Hubble constant as described below. More recently, SZE data has been used to determine cluster gas mass fractions which in turn have led to constraints on the universal matter density parameter  $\Omega_M$ . While these applications are of substantial interest, the availability of high quality SZE data offers the ability to learn a great deal more about clusters and cosmology.

Armed with data sets from multiple observables of a clusters, many parameters of interest, i.e., masses, gas mass fraction, electron temperature, Hubble constant, gas clumping factor, are often over-constrained. This will allow assumptions of the ICM structure to be tested, providing a much better understanding of galaxy clusters. In turn, this will lead to improvements in the precision with which cluster observations can be used to determine cosmological parameters.

For example, it is assumed that thermal pressure is the only significant form of support when the virial theorem is used to derive cluster masses. There is currently no compelling evidence against this assumption. A comparison of masses derived from the virial theorem (using X-ray, SZE or galaxy velocity dispersion data) and gravitational lensing should be able to test this assumption.<sup>17,18,19,20,16</sup>

As the precision with which we know cosmological parameters increases, the same calculations now used to derive the parameters can be turned around to solve for cluster properties. For example, the masses and electron temperatures of distant high redshift clusters ( $z > 0.8$ ) were determined directly from SZE observations without access to X-ray data,<sup>21</sup> based on the assumption that their gas mass fractions are consistent with the mean gas fraction derived from SZE and X-ray spectroscopic data for a sample of 18 high redshift clusters.<sup>22,23</sup> The ability to determine cluster temperatures and masses from only SZE data without access to X-ray data has important consequences for the analysis of deep SZE surveys of the distant universe.

SZE surveys for distant clusters will provide a powerful new tool for cosmological studies. As discussed below, SZE surveys will provide a direct view of the distant universe by finding all clusters regardless of redshift; should clusters exist at redshifts much higher than currently predicted they will be found by SZE surveys, but missed in even the deepest X-ray observations planned. The surveys will provide a large sample of clusters which can be used, for example, to

refine the determination of the Hubble constant. A powerful use of SZE surveys will be to place tight constraints on  $\Omega_M$  and  $\Omega_\Lambda$ , and for sufficiently large samples, on the equation of state of the dark energy from the analysis of the evolution of the number density and mass distribution of the survey yields.

### 3.1 Distance Determinations, Hubble constant

Several years after the SZE was first proposed<sup>1,2</sup> it was recognized that the distance to a cluster, and therefore the Hubble constant, could be determined with a measure of its SZE and its X-ray emission<sup>24,25,26,27,28,29</sup>

The distance can be determined by exploiting the different density dependencies of the SZE and X-ray emissivity. The SZE is proportional to first power of the density:  $\Delta T \sim \int dl n_e T_e$ , where  $dl$  is along the line of sight,  $n_e$  is the electron density and  $T_e$  is the electron temperature. We define  $dl \equiv D_A d\zeta$  to relate  $D_A$  and an ‘angle’ along the line of sight to the angle subtended by the cluster on the sky. The X-ray emission is proportional to the second power of the density:  $S_{x0} \sim \int dl n_e^2 \Lambda_{eH}$ , where  $\Lambda_{eH}$  is the X-ray cooling function. The angular diameter distance is solved for by eliminating the electron density<sup>f</sup> yielding

$$D_A \propto \frac{(\Delta T_0)^2 \Lambda_{eH}}{S_{x0} T_{e0}^2} \frac{1}{\theta_c}, \quad (5)$$

where these quantities have been evaluated along the line of sight through the center of the cluster (subscript 0) and  $\theta_c$  refers to a characteristic scale of the cluster along the line of sight, whose exact meaning depends on the density model adopted.

We need to know (or assume) something about the geometry of the cluster to relate an observation of  $\theta_c^{sky}$  to the characteristic scale of the cluster along the line of sight,  $\theta_c$ . Typically, spherical symmetry is assumed for the cluster geometry since for a large sample of clusters one would expect  $\langle \theta_c^{l.o.s.} / \theta_c^{sky} \rangle = 1$ , at least in the absence of selection effects (e.g.,<sup>30</sup>). A survey of a few hundred clusters with redshifts extending beyond one would allow the technique to be used to trace the expansion history of the universe, providing a valuable independent check of the type Ia supernova results.<sup>31,32</sup> Such a survey is now observationally well within reach.

It should be noted that in the SZE determination of the distance to a cluster, it is assumed that the clumping factor  $C \equiv \langle n_e^2 \rangle^{1/2} / \langle n_e \rangle$ , equals unity. The derived Hubble constant will be a factor of  $C^2$  times larger than the true Hubble constant.

### 3.2 Cluster Peculiar Velocities

The line of sight velocity of a cluster with respect to the CMB rest frame, the peculiar velocity of the cluster, can be measured by separating the kinetic from the thermal SZE. From inspection of Fig. 1, it is clear that this is best done by observation at frequencies near the null of the thermal effect at  $\sim 218$  GHz.

Such measurements offer the ability to measure the peculiar velocity of clusters at high redshifts which could be used to constrain large scale gravitational perturbations to the Hubble flow. The intrinsic weakness of the effect makes it challenging to observe. Upper limits have been placed on the peculiar velocities of clusters,<sup>33,34</sup> but a clear detection of the kinetic effect has not yet been obtained. The kinetic SZE is a unique and potentially powerful cosmological tool as it provides the only known way to measure large scale velocity fields at high redshift. As discussed in section 4.1, contamination by CMB temperature fluctuations as well as other sources will make it difficult to determine accurately the peculiar velocity for a given cluster.

<sup>f</sup>Similarly, one could eliminate  $D_A$  in favor of the central density,  $n_{e0}$

It may be possible, however, to determine mean peculiar velocities on extremely large scales by averaging over many clusters.

### 3.3 Baryon mass fraction of clusters, $\Omega_M$ , and $T_e$

The total SZE flux from a cluster is simply proportional to the gas mass of the cluster weighted by the temperature of the gas ( $\int d\Omega \Delta T_{SZE} \sim M_{gas} \langle T_e \rangle D_A^{-2}$ ). Combined with a measure of the total gravitating mass of the cluster, one can estimate the fraction of the mass contained in the ICM. The ICM contains most of the baryons confined to the cluster potential with roughly an order of magnitude more baryonic mass than that observed in the galaxies themselves.<sup>35,36</sup> The gas mass fraction is therefore a reasonable estimate of the baryonic mass fraction of the cluster. Furthermore, it is not believed that segregation between baryonic and non-baryonic mass occurs on the scales from which massive clusters condense  $\sim 1000 \text{ Mpc}^3$ , although a small fraction of baryons ( $\sim 15\%$ ) are likely lost during the cluster formation process.<sup>35</sup> The baryonic mass fraction of clusters therefore should reflect the universal mass fraction of baryons to total matter,  $\Omega_B/\Omega_M$  where  $\Omega \equiv \rho/\rho_c$  and  $\rho_c$  is the critical density of the universe.

With knowledge of  $\Omega_B$ , the measured gas mass fraction of a cluster of galaxies leads to an estimate of the universal matter density,  $\Omega_M$ . Recent reanalysis of BBN predictions with careful uncertainty propagation<sup>37,38</sup> along with recent D/H measurements in Ly $\alpha$  clouds<sup>39,40</sup> constrain the baryon density to be  $\Omega_B h_{100}^2 = 0.019 \pm 0.0012$  at 68% confidence. An additional independent determination of  $\Omega_B h^2$  will soon be provided by precision measurements of the intrinsic CMB anisotropy angular power spectrum.

The gas mass is measured directly by observations of the SZE provided the electron temperature is known. The total gravitating mass can be determined through hydrostatic equilibrium with knowledge of the distribution of the gas and, again, knowledge of the electron temperature. The SZE derived gas mass fraction will therefore be proportional to  $\Delta T_{SZE}/T_e^2$ . Alternatively, the total gravitating mass can be determined from measurement of strong lensing (on small scales) or from weak lensing (on large scales).

A comparison of SZE derived gas mass and lensing total gravitating mass is particularly interesting as both are measures of the projected mass distribution. It has been shown that the gas mass fraction can be determined from the analysis of SZE and lensing measurements without need to parameterize the ICM distribution.<sup>41</sup> Furthermore, by comparing this mass fraction with one derived using the virial theorem, it is possible to solve for the ICM electron temperature.<sup>41</sup>

Cluster gas mass fractions can also be determined from cluster X-ray emission in the same manner as from SZE measurements. There are several important differences, however. First the X-ray emission, being proportional to the ICM density squared, is more susceptible to clumping of the gas,  $C$ . The X-ray derived gas mass is essentially insensitive to the electron temperature, while the SZE derived gas mass is proportional to  $1/T_e$ .

Currently, X-ray data for low redshift clusters is of exceptional quality, far surpassing SZE data. X-ray based gas mass fractions have been measured to cluster radii of 1 Mpc or more.<sup>42,43,44,45,46</sup> In an X-ray flux-limited sample of 45 clusters,<sup>46</sup> the mean cluster gas mass fraction within approximately the virial radius was found to be  $(0.0749 \pm 0.0005)h_{100}^{-3/2}$ . The quality of SZE images is improving quickly as discussed in section 4, and already the SZE and X-ray data for high redshift clusters are of comparable quality (see Sec. 4).

### 3.4 Cosmology with SZE Surveys

Perhaps the most powerful use of the SZE for cosmology will be to probe the high redshift universe. Sensitive, non-targeted surveys of large regions of the sky for the SZE will provide an accurate inventory of clusters independent of their redshift.

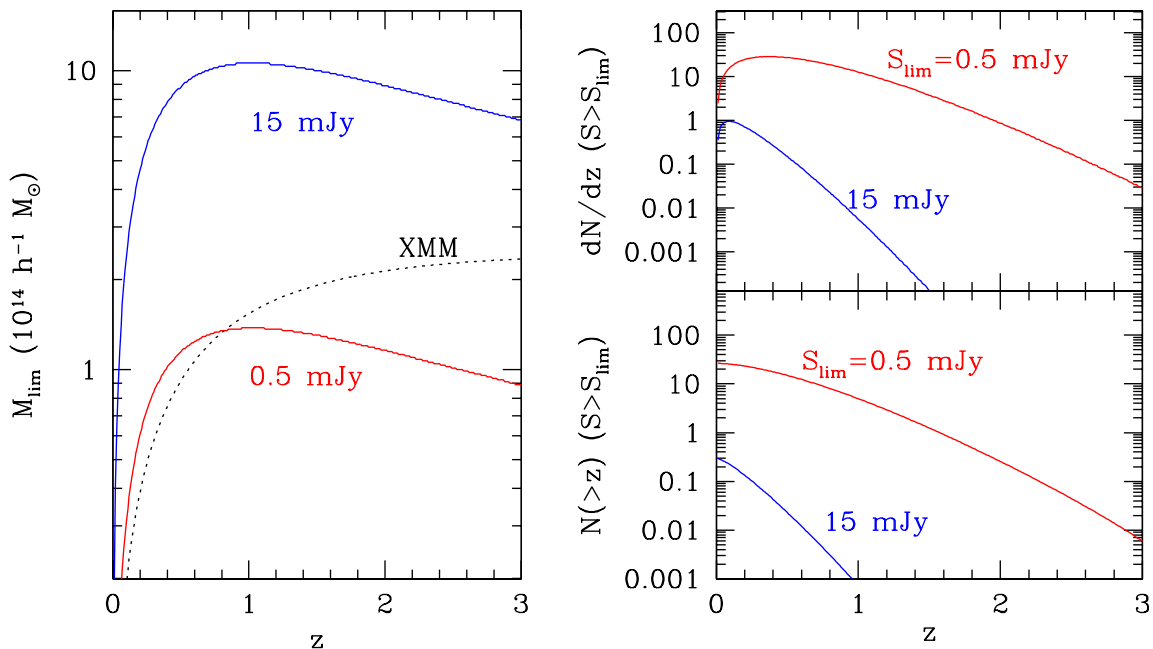


Figure 2: Left: Mass limits as a function of redshift for a typical wide-field type of survey (sensitivity limit of  $\sim 15$  mJy at 30 GHz) and for a typical deep survey ( $\sim 0.5$  mJy). The approximate XMM serendipitous survey limit is also shown. Right: Differential (top) and cumulative (bottom) counts per square degree as a function of redshift for two SZE surveys shown at left, assuming a  $\Lambda$ CDM cosmology.<sup>3</sup>

The evolution of the abundance of galaxy clusters is a sensitive probe of cosmology. Measurements of the clusters masses and number density as a function of redshift can be used to constrain the matter density,  $\Omega_M$ ,<sup>47,48,49,4</sup> and, for sufficiently large samples, the equation of the state of the dark energy.<sup>4</sup> X-ray surveys have already been used to constrain  $\Omega_M$ , but they have been limited by sample size and their reduced sensitivity to high redshift clusters. SZE surveys offer the attractive feature of probing the cluster abundance at high redshift as easily as the local universe.

The sensitivity of a SZE survey is essentially a redshift independent mass limit (see Fig. 2).<sup>50,51,3</sup> The integrated SZE for a cluster is proportional the temperature weighted mass of the cluster and inversely to the square of the angular diameter distance,  $\Delta T_{SZE} \propto \langle T_e \rangle M_{virial}/D_A^2$ . At low redshift the mass detection threshold of a SZE survey increases with  $D_A^2$ . At high redshift,  $z \sim 1$ , the mass threshold flattens and even begins to decrease. This is due to two effects: 1)  $D_A(z)$  begins to flatten and 2) for a given virial mass,  $M_{virial}$ , high redshift clusters will be denser and hotter (due to the increase in the matter density) leading to a stronger SZE flux.

SZE surveys can be broadly grouped into two types of surveys: large area, relatively shallow surveys, similar to what can be expected with the Planck Surveyor Satellite, or relatively small, deep surveys, such as those expected with upcoming ground-based efforts. In Fig. 2 we show the approximate expected limiting mass for the two types of surveys, assuming a simple limit on the integrated flux density of 15 mJy at 30 GHz as expected for Planck and 0.5 mJy for deep ground-based surveys. We use 30 GHz as an arbitrary normalizing frequency; to convert to integrated Compton  $y$ -parameter use  $S_{30} = 12.7(y/arcmin^2)$  Jy. As a comparison, we have also shown an approximate mass limit for an XMM serendipitous survey,<sup>52</sup> assuming a simple X-ray flux limit. A deep SZE survey will be able to probe somewhat lower masses at redshifts past  $z \sim 1$ , which promises to be a very interesting regime.

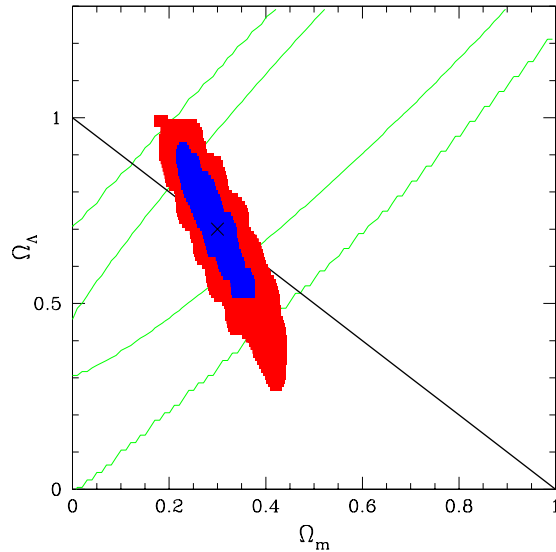


Figure 3: A simulation of the constraints in the  $\Omega_M$ - $\Omega_\Lambda$  plane which should be possible from the analysis of a SZE survey covering 12 square degrees in which all clusters above  $10^{14}h_{100}^{-1} M_\odot$  are detected. The input cosmology is  $\Omega_M = 0.3$  and  $\Omega_\Lambda = 0.7$ . The blue region corresponds to the 68% confidence region, red to 95%. The value of  $\sigma_8$  has been marginalized over rather than kept fixed. The diagonal ellipses are the current constraints based on the analyses of type Ia supernovae at 68% and 95% confidence.<sup>31,32</sup> The diagonal line at  $\Omega_M + \Omega_\Lambda = 1$  is for a flat universe as suggested by recent CMB anisotropy measurements.<sup>53,54,55</sup>

In the right panels of the Fig. 2, we show the expected counts per square degree for a  $\Lambda$ CDM model ( $\Omega_m = 0.3, \Omega_\Lambda = 0.7, h = 0.65, \sigma_8 = 1$ ). A deep SZE survey can expect to find roughly one cluster per square degree with  $z > 1.5$ . On the other hand, even though a shallow survey has a relatively high mass limit, a survey that covers half the sky would find roughly 10000 clusters, many of which would be near enough to appear in the Sloan Digital Sky survey.

There are many possible uses of a cluster catalog extending to high redshift with a simple selection function. An important use would be to use the cluster abundance and its redshift evolution as a strong test of cosmological parameters<sup>4</sup> and the structure formation paradigm in general. In Fig. 3 we show the expected constraints in the  $\Omega_M$ - $\Omega_\Lambda$  plane based on the analysis of a hypothetical deep SZE survey<sup>56,3</sup> covering 12 square degrees in which all clusters above  $10^{14}h_{100}^{-1} M_\odot$  are detected and for which redshifts are known. The input cosmology is  $\Omega_M = 0.3$  and  $\Omega_\Lambda = 0.7$ . The blue region corresponds to the 68% confidence region, red to 95%. The value of  $\sigma_8$  has been marginalized over rather than kept fixed. Obtaining redshifts for the clusters found in such a survey would be greatly facilitated by coordinating the selection of the SZE fields with those of deep optical surveys. Redshifts would then be available for all clusters with  $z \lesssim 1$ . Deep follow-up optical and infrared observations could then be targeted at the resulting list of high redshift clusters.

Another use of the resulting catalog is to probe the redshift evolution of the intracluster medium, perhaps seeing the effects of feedback from galaxy formation<sup>57</sup> out to  $z \sim 2$ . In fact, so little is currently known about relatively low-mass clusters at high redshift that it is difficult to predict the most important uses of such a catalog.



## 4 Observations of the Sunyaev-Zel'dovich Effect

In the twenty years following the first papers by Sunyaev and Zel'dovich<sup>1,2</sup> there were few firm detections of the SZE despite a considerable amount of effort.<sup>58</sup> Over the last several years, however, observations of the effect have progressed from low signal to noise detections and upper limits to high confidence detections and detailed images. In this section we briefly review the state of SZE observations. The constraints on the cosmological parameters that have already been determined by existing SZE observations are discussed in the next section.

The dramatic increase in the quality of the observations is due to improvements both in low-noise detection systems and in observing techniques, usually using specialized instrumentation to carefully control the systematics that often prevent one from obtaining the required sensitivity. Such systematics include, for example, the spatial and temporal variations in the emission from the atmosphere and the surrounding ground, as well as gain instabilities inherent to the detector system used. To appreciate the importance of controlling these systematics, consider the theoretical sensitivity of a modestly sensitive radio receiver with a noise temperature<sup>9</sup> of 100 K and a detector bandwidth of 1 GHz; it would be  $3mKs^{-1/2}$ . Such a system should secure a detection of the SZE for a massive cluster within an hour or so. However, observations with far more sensitivity have failed to detect the SZE even after many hours of integration. Detector systems today typically have sensitivities around  $1mKs^{-1/2}$ . Clearly, the goal of all modern SZE instruments is control of systematics.

The observations must be conducted on the appropriate angular scales. Galaxy clusters are large objects with a characteristic scale size of order a Mpc. In any reasonable cosmology, a Mpc subtends an arcminute or more at any redshift; low redshift clusters will subtend a much larger angle, for example the angular extent of the Coma cluster ( $z = 0.0235$ ) is of order a degree (core radius  $\sim 10'$ ).<sup>59</sup> The detection of extended low surface brightness objects requires precise differential measurements made toward widely separated directions on the sky. On these large angular scales, offsets due to differential ground pick-up and atmospheric variations are difficult to control.

### 4.1 Sources of astronomical contamination and confusion

In designing an instrument for SZE observations, one needs to take into account several sources of possible contamination and confusion from astronomical sources. One such source is anisotropy of the CMB itself. For distant clusters with angular extents of a few arcminutes it is not a problem as the CMB anisotropy has been shown to be damped considerably on these scales.<sup>60,61,62</sup> For nearby clusters, or for searches for distant clusters using large beams of order  $10'$  or more, the intrinsic CMB anisotropy must be considered. The unique spectral behavior of the thermal SZE can be used to separate it from the intrinsic CMB in these cases. Note, however, that for such cases it will not be possible to separate the kinetic SZE effects from the intrinsic CMB anisotropy without relying on the very small spectral distortions of the kinetic SZE due to relativistic effects.

Historically, the major source of contamination in the measurement of the SZE has been radio point sources. It is obvious that emission from point sources located along the line of the sight to the cluster could fill in the SZE decrement, leading to an underestimate. The radio point sources are variable and therefore must be monitored. Radio emission from the cluster member galaxies, often from the central CD galaxy, is often the largest source of radio point source contamination, at least at high radio frequencies.<sup>63</sup> The flux,  $S_\nu$ , of a radio source typically has a spectral index of  $\alpha \sim 0.7$  for  $S_\nu = \nu^{-\alpha}$ . In the RJ limit, the SZE flux is proportional to  $\nu^2$

---

<sup>9</sup>the required input power expressed in temperature units that would result in the same measured output noise power of an equivalent but noiseless system

and therefore point sources are much less of an issue at higher radio frequencies.

While it is most likely that insufficient attention to radio point sources would lead to the underestimate of the SZE effect, it could also lead to an overestimate. The most obvious example is if unaccounted point sources are in the reference fields surrounding the cluster. An effect due to gravitational lensing has also been pointed out for low frequency observations where the flux from many point sources must be taken into account before a reliable measure of the SZE can be made. Essentially, the added efficiency of detecting point sources toward the center of the cluster due to gravitational lensing could lead to an overestimate of the SZE decrement.<sup>64</sup> This effect should be negligible at frequencies greater than roughly 30 GHz.

At frequencies near the null of the thermal SZE and higher, dust emission from extragalactic sources as well as dust emission from our own galaxy must be considered. Over the frequencies of interest, dust emission rises steeply as  $\nu^{2+\beta}$ , where  $\nu^\beta$  is the scaling of the dust opacity with  $1 < \beta < 2$ . Consider the dusty extragalactic sources that have been found toward massive galaxy clusters with the SCUBA bolometer array.<sup>65</sup> Sources with 350 GHz (850  $\mu m$ ) fluxes greater than 8 mJy are common and all clusters surveyed had multiple sources with fluxes greater than 5 mJy. A 10 mJy source at 350 GHz corresponds to a contaminant of the CMB of magnitude  $\Delta T_{CMB} = 345 \mu K$  for 1' beam, or a Compton  $y$ -parameter of  $6 \times 10^{-5}$ . The same source scaled to 270 GHz, assuming a dust opacity law of  $\nu^{1.5}$ , leads to  $\Delta T_{CMB} = 95 \mu K$  for a 1' beam and a  $y$ -parameter of  $4 \times 10^{-5}$ . Scaling to the SZE thermal null at 218 GHz gives 5 mJy which corresponds to a  $\Delta T_{CMB} = 41 \mu K$  for a 1' beam. This in turn translates directly to an uncertainty in a measurement of the cluster peculiar velocity (Eq. 4); for a massive cluster with an optical depth of 0.01 ( $y$ -parameter of  $2 \times 10^{-4}$  and an electron temperature of 10 keV), 41  $\mu K$  corresponds to a peculiar velocity of 450 km s<sup>-1</sup>. The contamination is more severe for less massive clusters with the dependence scaling as  $\Delta v_{pec} \propto \tau_e^{-1} \propto R^2/M \propto M^{-1/3} \propto T_e^{-1/2}$ .

As with SZE observations in the radio, high frequency observations also need to consider the effects of point sources and require either high dynamic angular range, large spectral coverage, or both, to separate the point source emission from the SZE.

#### 4.2 Single Dish Observations

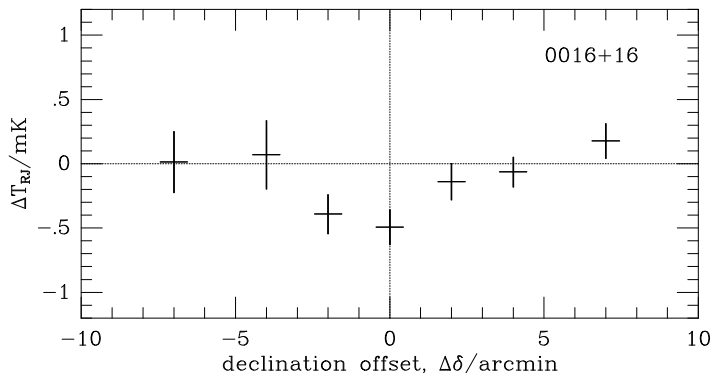


Figure 4: A measurement of the SZE profile across the cluster CL 0016+16 obtained with the OVRO 40 m telescope.<sup>58,66</sup> The observed profile provided confidence in the reliability of this early detection.

The first measurements of the SZE were made with single dish radio telescopes at cm wavelengths. Advances in detector technology made these measurements possible, although early observations appear to have been plagued by systematic errors which led to irreproducible and inconsistent results. Eventually, successful detections were obtained, although the reported

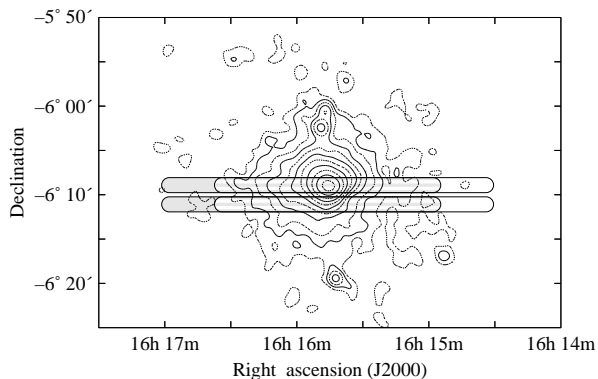


Figure 5: The drift scans of the two detector rows of the SuZIE instrument superimposed on the X-ray surface brightness contours for Abell 2163. The two sets of scans, white and grey, correspond to two sets of measurements that differed only in the position at which the drift scan started.<sup>76</sup>

results show considerable scatter reflecting the difficulty of these measurements. During this period, the pioneering work of Birkinshaw and collaborators with the OVRO 40 meter telescope stands out for its production of results which served to build confidence in the technique.<sup>67,68</sup> One of the first measurements of the profile of the SZE decrement across a galaxy cluster is shown in Fig. 4.<sup>66,69,58</sup>

All observations sensitive enough to observe the SZE are differential. The primary issue for single dish observations is how to switch the beam on the sky without introducing systematics comparable to the SZE. This beam switching can be accomplished in several ways, including but not limited to Dicke switching between feeds and chopping mirrors which switch or sweep the beam on the sky. With a single dish telescope, modulation of the beam sidelobes can lead to an offset. This offset can be removed if it remains stable enough that it can be measured on a portion of the sky without the cluster. However, as a source is tracked over the course of an evening, temperature variations of the optics and features on the ground can cause the offset to change. Therefore, it has become common practice to observe leading and trailing fields with the same position with respect to the ground as for the cluster observation. In this way, any constant or linear drift in offset can be removed at the price of observing efficiency and sensitivity. This technique has been used successfully with the OVRO 5 meter telescope at 32 GHz to produce reliable detections of the SZE in several intermediate redshift clusters.<sup>59,70</sup> The SEST 30 meter and IRAM 15 meter telescopes have been used with bolometric detectors at 140 GHz and chopping mirrors to make significant detections of the SZE in several clusters.<sup>72,73</sup> In the Sunyaev-Zel'dovich Infrared Experiment (SuZIE) on the CSO submillimeter telescope, pixels in the six element 142 GHz bolometer array are electronically differenced by reading them out in a differential bridge circuit.<sup>74</sup> Differencing in this way makes the experiment insensitive to temperature and amplifier gain fluctuations that produce  $1/f$  noise. This increased low frequency stability allows SuZIE to observe in a drift scanning mode where the telescope is fixed and the rotation of the earth moves the beams across the sky. Using this drift scanning technique, the SuZIE experiment has produced high signal to noise strip maps of the SZE emission in several clusters.<sup>33,75</sup> An example of a SuZIE scan pattern and strip map are shown in Fig. 5 and Fig. 6, respectively.

Because of the high sensitivity of bolometric detectors at millimeter wavelengths, single dish experiments are ideally suited for the measurement of the SZE spectrum. By observing at several millimeter frequencies these instruments are able to separate the thermal and kinetic SZE from atmospheric fluctuations and sources of astrophysical confusion. One of the first steps to

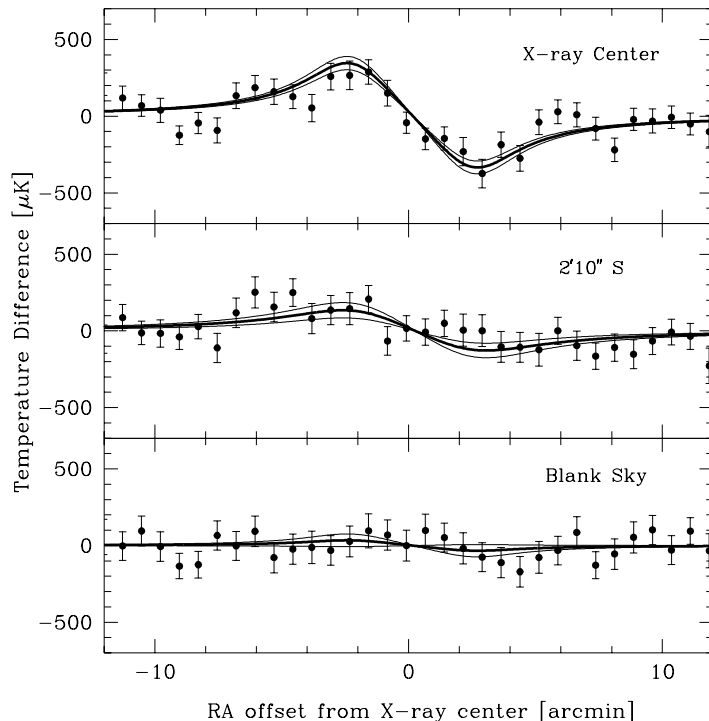


Figure 6: Coadded SuZIE drift scans across the X-ray center of Abell 2163,  $2'10''$  to the South, and on a patch of sky believed to be free of sources. The line is the predicted SZE differential signal calculated from the X-ray data assuming isothermal ICM gas, which has been scaled to fit the data.<sup>76</sup>

realizing this goal is the measurement of the SZE as an increment. So far, there have been only a few low signal to noise detections at a frequency of approximately 270 GHz. The main reason for the lack of detection is the increased opacity of the atmosphere at higher frequencies, and these measurements typically require the lowest opacity and most stable atmosphere. Holzapfel et al. (1997)<sup>33</sup> report a detection of A2163 with the SuZIE instrument at 270 GHz. Observations by Andreani et al. (1996)<sup>73</sup> claim detections of the SZE increment in two clusters, although observations of third cluster appear to be contaminated by foreground sources or systematic errors.<sup>77</sup>

Single dish observations of the SZE are just beginning to reach their potential and the future is promising. The development of large format millimeter wavelength bolometer arrays will increase the mapping speed of current SZE experiments by orders of magnitude. The first of this new generation of instruments is the BOLOCAM 151 element bolometer array<sup>78,79</sup> which has just completed a engineering run at the CSO and will begin observations in May 2001. BOLOCAM will observe in drift scanning mode and produce differences between bolometer signals in software. To the extent that atmospheric fluctuations are common across the array, it will be possible to realize the intrinsic sensitivity of the detectors. Operating from astronomical sites with stable atmospheres and low precipitable water vapor, future large format bolometer arrays have the potential to produce high signal to noise SZE images and search for distant SZE clusters with unprecedented speed.

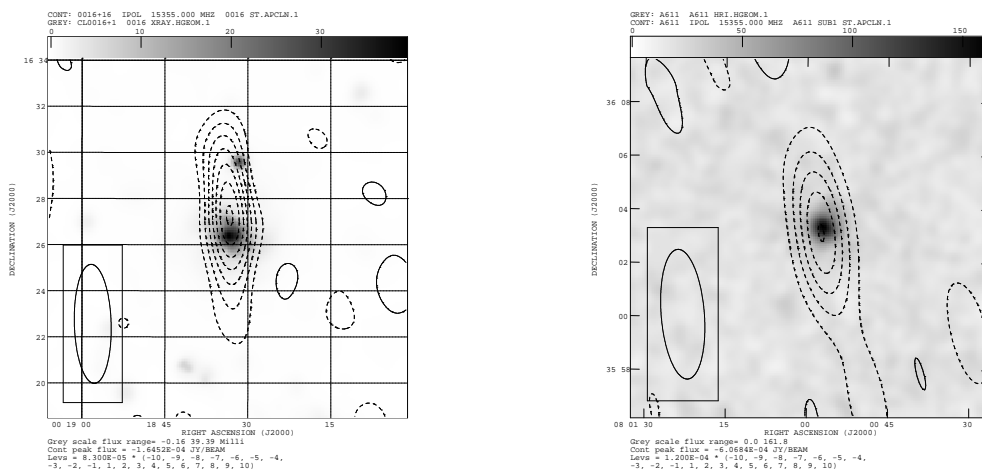


Figure 7: Ryle Telescope (RT) images (contours) superposed on ROSAT PSPC images (greyscale) of the SZE effect in two clusters, CL 0016+16 at  $z=0.54$  and Abell 611 at  $z=0.288$ . A611 has only 1/6 the X-ray luminosity of CL 0016+16. The ellipses show the FWHM of the RT synthesized beam, which is strongly elongated in both cases.<sup>88</sup>

### 4.3 Interferometric observations

The stability and spatial filtering inherent to interferometry has been exploited to make high quality images of the SZE.<sup>80,81,82,83,84,85,21,22,86,87,23</sup> We first review the basic operating principles of an interferometer.

The ‘beam’ of a two-element interferometer – all arrays can be thought of as a collection of  $n(n-1)/2$  two-element interferometers – is essentially a cosine corrugation on the sky, analogous to a two slit interference pattern and thus provides simultaneous differential measurements. The interferometer effectively multiplies the sky brightness at the observing frequency by a cosine, integrates the product and outputs the time average amplitude of the product. In practice the signal path is split and a 90 degree relative phase shift is inserted into one path so that the output of the interferometer is the complex Fourier transform of the sky brightness at a spatial frequency given by  $B/\lambda$ , where  $B$  is the component of the vector connecting the two telescopes (the baseline) oriented perpendicular to the source. Of course, a range of baselines are actually being used at any one time due to the finite size of the apertures of the individual array elements; this simply reflects that the sky has been multiplied by the gain pattern (beam) of the individual telescopes or, equivalently, that the Fourier transform measured is the transform of the true sky brightness convolved with the transform of the beam of an array element.<sup>h</sup>

The transformed beam is the auto-convolution of the aperture; it is identically zero beyond the diameter of the telescopes expressed in wavelengths. The interferometer is therefore only sensitive to angular scales (spatial frequencies) near  $B/\lambda$ . It is insensitive to gradients in the atmospheric emission or other large scale emission features. There are several other features which allow an interferometer to achieve extremely low systematics. For example, only signals which correlate between array elements will lead to detected signal. For most interferometers, this means that the bulk of the sky noise for each element will not lead to signal. Amplifier gain instabilities for an interferometer will not lead to large offsets or false detections, although if severe they may lead to somewhat noisy signal amplitude. To remove the effects of offsets or

<sup>h</sup>the beam here is often referred to as the primary beam, or gain envelope, of the interferometer and sets the field of view of the interferometer at  $\approx \lambda/D$  where  $D$  is the diameter of the telescope.

drifts in the electronics as well as the correlation of spurious (non-celestial) sources of noise, the phase of the signal received at each telescope is modulated before the correlator and then the proper demodulation is applied to the output of the correlator.

Lastly, the spatial filtering of an interferometer allows the emission from radio point sources to be separated from the SZE emission (e.g., see Fig. 9). This is possible because at high angular resolution ( $\sim 10''$ ) the SZE contributes very little flux. This allows one to use long baselines – which give high angular resolution – to detect and monitor the flux of radio point sources while using short baselines to measure the SZE. Nearly simultaneous monitoring of the point sources is important as they are often time variable. The signal from the point sources is then easily removed, if they are not too strong, from the short baseline data which are sensitive to the SZE. In practice, the fluxes of the point sources are fitted jointly with the SZE signal.

For the reasons given above, interferometers offer an ideal way to achieve high brightness sensitivity for extended low-surface brightness sources, at least at radio wavelengths. Most interferometers, however, were not designed for imaging low-surface brightness sources. Interferometers are traditionally built to obtain high angular resolution with large individual elements for maximum sensitivity to small scale emission. Galaxy clusters, on the other hand are large objects. As a result, special purpose interferometric systems have been built for imaging the SZE. All of them have taken advantage of low-noise HEMT amplifiers<sup>89</sup> to achieve high sensitivity.

The first interferometric detection<sup>80</sup> of the SZE was obtained with the Ryle Telescope.<sup>80,81,83,90</sup> It is composed of eight 13 m telescopes located in Cambridge, England operating at 15 GHz with East-West configurations. Images of the SZE toward two clusters obtained with the Ryle Telescope are shown in Fig. 7; the East-West array configuration of the telescope lead to North-South elongated synthesized beams.

The OVRO and BIMA SZE imaging project<sup>82,56,22,85,86,87,23,21</sup> uses 30 GHz (1 cm) low noise receivers mounted on the OVRO<sup>*i*</sup> or BIMA<sup>*j*</sup> mm-wave arrays in California. A subset of the 35 images obtained to date from the OVRO and BIMA SZE imaging project is shown in Fig. 8. The OVRO and BIMA arrays support two dimensional configurations of the telescopes, including extremely short baselines, allowing good synthesized beams for imaging the SZE of clusters at declinations greater than  $\sim -20$  degrees.

Fig. 8 also clearly demonstrates the independence of the SZE on redshift. The clusters have similar X-ray luminosities, but span a factor of five in redshift. As can be seen, the strength of the SZE for each cluster is similar.

Point sources were removed from a large fraction of the SZE images shown in Figs. 7 and 8. The interferometers image the point sources simultaneously with the SZE by using telescope configurations that include a large range of baseline lengths. The point sources are identified in a straight forward manner since their detected flux is independent of baseline length. An example of the effectiveness of the removal of bright point sources is illustrated in Fig. 9 where we show BIMA data of the extremely X-ray luminous cluster RX J1347-1145 at  $z = 0.45$ . As shown in the right panel, a strong (10.7 mJy) point source is observed toward the center of the cluster. The SZE of this cluster has been the target of single dish observations with the Nobeyama 45 m telescope at 21 GHz, 43 GHz,<sup>91</sup> and 150 GHz,<sup>92</sup> with the DIABOLO bolometric system on the IRAM 30 m at 140 GHz (2.1 mm) and 250 GHz (1.2 mm)<sup>93</sup> and with the SCUBA bolometric array on the JCMT 15 m telescope at 350 GHz.<sup>91</sup> These observations were not able to account for the contaminating flux of the radio point source without adding considerable uncertainty to the magnitude and morphology of the SZE. The interferometric observations presented here easily separated the point source emission from the SZE. A recent high resolution image made with the DIABOLO instrument on the IRAM telescope was also able to distinguish the point

<sup>*i*</sup>An array of six 10.4 m telescopes located in the Owens Valley, CA and operated by Caltech

<sup>*j*</sup>An array of ten 6.1 m mm-wave telescopes located at Hat Creek, California and operated by the Berkeley-Illinois-Maryland-Association

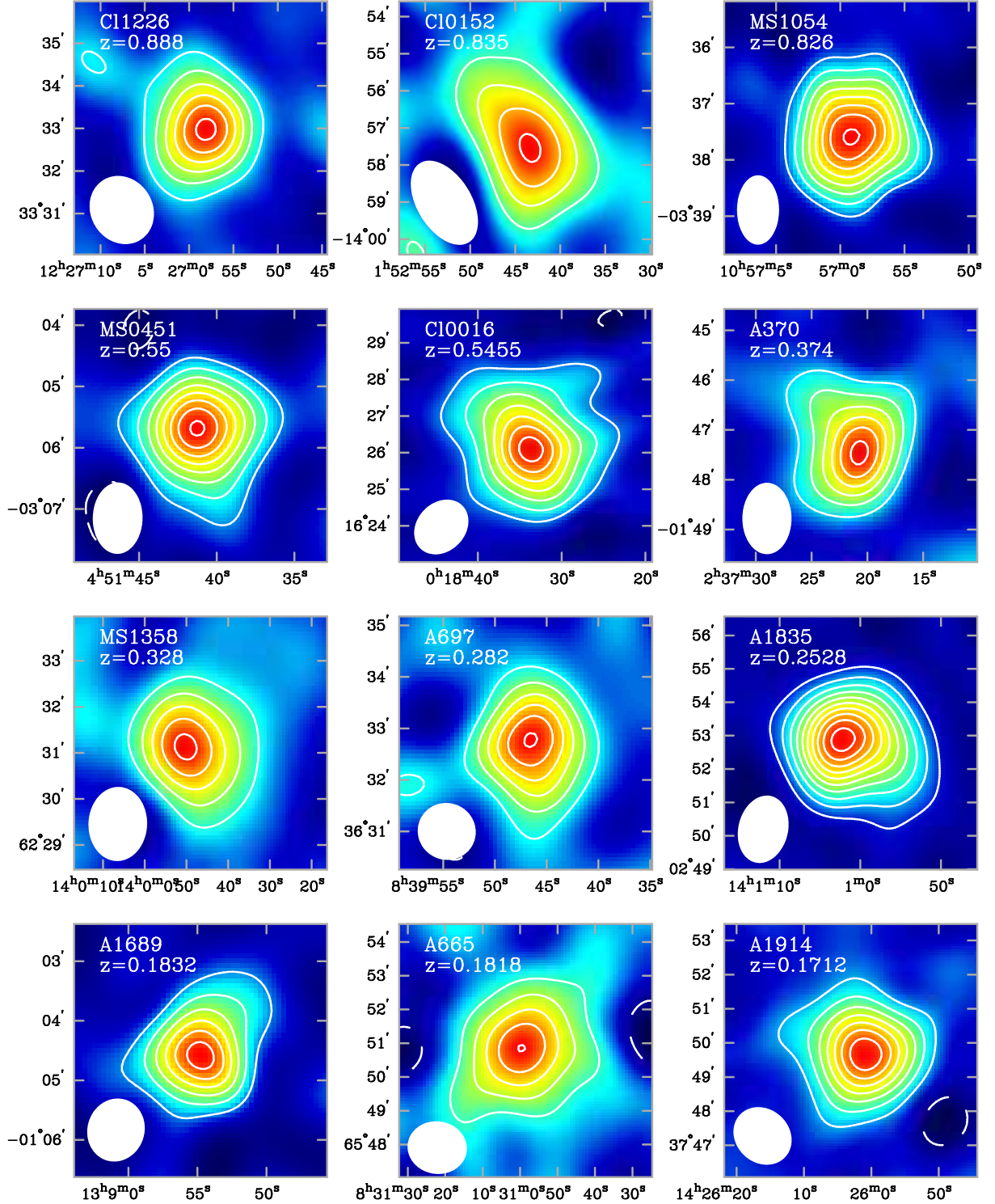


Figure 8: Deconvolved interferometric SZE images for a sample of galaxy clusters over a large redshift range ( $0.17 \leq z \leq 0.89$ ). The contours are multiples of  $2\sigma$  and negative contours are shown as solid lines. The FWHM ellipse of the synthesized beam is shown in the lower left corner of each panel. The noise level  $\sigma$  ranges from  $20\mu\text{K}$  to  $40\mu\text{K}$  for the clusters shown.

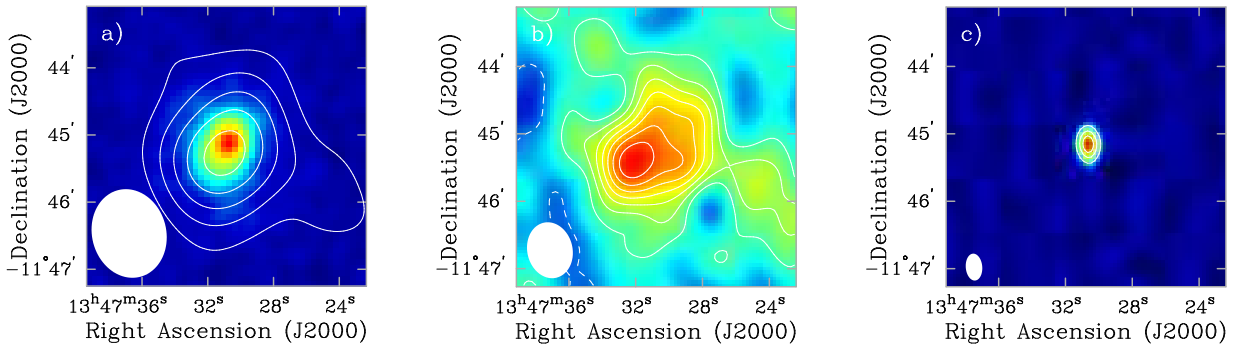


Figure 9: BIMA deconvolved interferometric images of the SZE of galaxy cluster RXJ1347-11 emphasizing different spatial scales. The FWHM ellipse of the synthesized beam is shown in the lower left corner of each panel. (a) Point source subtracted SZE image (contours) overlaid on ROSAT X-ray image (false color). The contours are multiples of  $185\mu\text{K}$  ( $\sim 2\sigma$ ), and negative contours are shown as solid lines. A  $1500\lambda$  half-power radius Gaussian taper was applied resulting in a  $63'' \times 80''$  synthesized beam. The X-ray image is HRI raw counts smoothed with a Gaussian with  $\sigma = 6''$  and contains roughly 4000 cluster counts. (b) Higher resolution point source subtracted SZE image (both contours and false color). A  $3000\lambda$  half-power radius Gaussian taper was applied resulting in a  $40'' \times 50''$  synthesized beam. The contours are multiples of  $175\mu\text{K}$  ( $\sim 1\sigma$ ) (c) Image of the point source made using projected baselines greater than  $3000\lambda$ . This map has a synthesized beam of  $15'' \times 24''$  and a rms of  $\sim 275\mu\text{Jy beam}^{-1}$  ( $1200\mu\text{K}$ ) sensitivity. The contours are multiples of  $10\sigma$ .

source emission from the SZE.<sup>94</sup>

The Ryle, OVRO, and BIMA SZE observations are insensitive to the angular scales required to image low redshift clusters,  $z < 0.1$ . Recently, however, the Cosmic Background Imager (CBI)<sup>96</sup> has been used to image the SZE in a number of nearby clusters. The CBI is composed of thirteen 0.9 m telescopes mounted on a common platform with baselines spanning 1 m to 6 m. Operating in ten 1 GHz channels spanning 26 - 36 GHz, it is sensitive to angular scales spanning  $3'$  to  $45'$ . In Fig. 10 we show a CBI image of the SZE toward Abell 401 at redshift 0.07.<sup>95</sup> As for single dish observations, data from observations of leading and trailing fields offset by 12.5 minutes in Right Ascension have been subtracted from the CBI cluster image to remove contamination from ground emission.

## 5 Current Status of Cosmological Constraints from SZE measurements

Current SZE observations are of sufficient quality that already significant constraints on cosmological parameters have been obtained.

### 5.1 Hubble Constant

As outlined in section 3.1, by analyzing a measurement of the SZE for a cluster in combination with its X-ray properties, one can solve for the angular diameter distance to the cluster. The Hubble constant is then easily computed with knowledge of the cluster redshift.

The beauty of this technique for measuring the Hubble constant is that it is completely independent of other techniques, and that it can be used to measure distances at high redshifts. While the method depends only on well understood properties of fully ionized plasmas, there are several sources of uncertainty in the derivation of the Hubble constant for any particular cluster. The largest uncertainty is the assumption that the cluster size along the line of sight



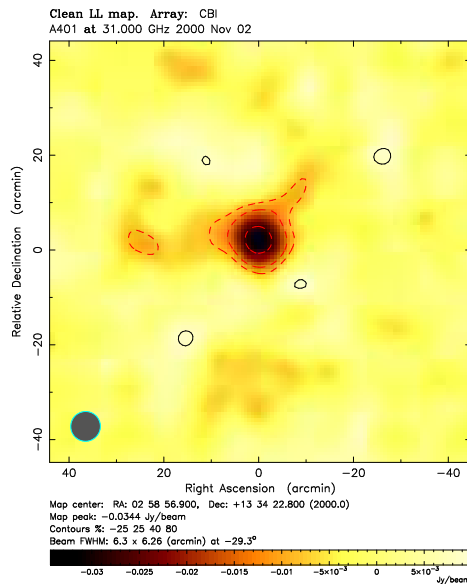


Figure 10: An image of the SZE toward Abell 401 obtained with the Cosmic Background Imager. The FWHM resolution is  $6.3' \times 6.3'$ . The contour levels are at -25, 25, 40, and 80% of the peak level of  $-34.2$  mJy per beam which corresponds to a brightness temperature of  $305\mu\text{K}$ . The noise level is  $20\mu\text{K}$ .<sup>95</sup>

is comparable to its size in the plane of the sky. For this reason it is desirable to use a large survey of clusters to determine  $H_o$ .

The error budget in the determination of the Hubble constant is also particularly sensitive to the electron temperature and measured SZE as it depends on the square of these quantities, i.e.,

$$H_o \propto \frac{S_X T_e^2}{(\Delta T_{SZE})^2} \quad (6)$$

where  $S_X$  is the X-ray intensity. Eq. 6 also illustrates the sensitivity of the SZE Hubble constant determination to the *absolute calibration* of the X-ray and SZE observations. Currently the best absolute calibration of SZE observations is  $\sim 2.5\%$  at 68% C.L. based on observations of the brightness of the planets, usually Mars and Jupiter.<sup>22,99</sup> This translates into a 5% systematic uncertainty shared by nearly all of the SZE measurements made to date. Efforts are now underway to reduce this uncertainty to the 1% level (2% in  $H_o$ ). Uncertainty in the X-ray intensity scale also adds another shared uncertainty as nearly all of the reported SZE Hubble constant determinations use data from the ROSAT satellite. The accuracy of the ROSAT intensity scale is debated, but a reasonable estimate is believed to be  $\sim 10\%$ . It is hoped that the calibration of the Chandra and XMM-Newton X-ray telescopes will greatly reduce this uncertainty.

The current status of SZE determined distances is summarized in Fig. 5.1 along with the theoretical  $D_A$  relation for three different cosmologies assuming  $H_0 = 60 \text{ km s}^{-1} \text{ Mpc}^{-1}$ . It is clear that SZE determined distances are beginning to trace the shape of the theoretical angular diameter distance relation. Excluding results from the BIMA and OVRO SZE project, there are currently 16 SZE determined distances to 14 different clusters for which reasonably high signal to noise SZE data and X-ray data exist. We are currently analyzing the subset (17 clusters) of the 35 galaxy clusters imaged with OVRO and BIMA SZE system for which good X-ray data exists, roughly doubling the number of direct distances to galaxy clusters (10 of which have no other SZE determined distance estimates). Preliminary results from 14 of these clusters can be found in the article by Reese et al. in this volume.<sup>104</sup>

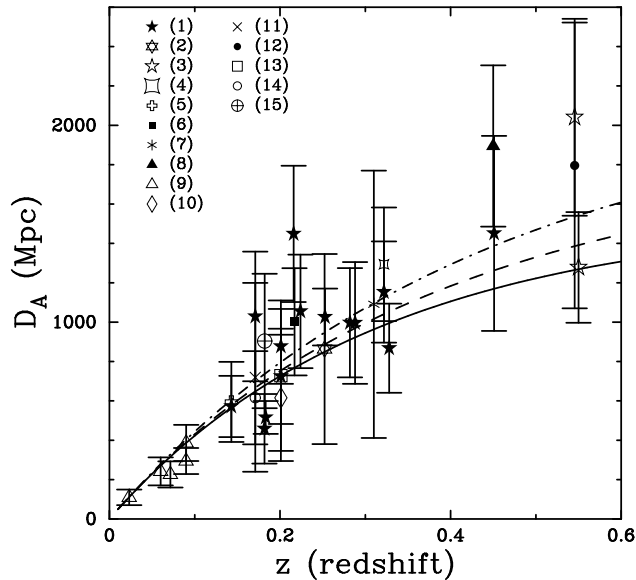


Figure 11: SZE determined distances versus redshift. Also plotted is the theoretical angular diameter distance relation for three different cosmologies, assuming  $H_0 = 60 \text{ km s}^{-1} \text{ Mpc}^{-1}$ . References: (1)<sup>97</sup>, (2)<sup>75</sup>, (3)<sup>87</sup>, (4)<sup>85</sup>, (5)<sup>90</sup>, (6)<sup>98</sup>, (7)<sup>77</sup>, (8)<sup>91</sup>, (9)<sup>99,70,59</sup>, (10)<sup>100</sup>, (11)<sup>101</sup>, (12)<sup>102</sup>, (13)<sup>76</sup>, (14)<sup>103</sup>, and (15)<sup>58</sup>.

A fit to all the SZE determined distances implies  $H_0 = 63 \pm 3 \text{ km s}^{-1} \text{ Mpc}^{-1}$  for an  $\Omega_M = 0.3$  and  $\Omega_\Lambda = 0.7$  cosmology, where the uncertainty is the formal statistical uncertainty at 68% confidence. We caution that the statistical uncertainties are difficult to interpret and the systematics are difficult to ascertain because many of these distances share systematics. Though the systematics are difficult to determine precisely, they contribute roughly a 30% uncertainty. Many of the clusters are at high redshift where the geometry of the universe affects the best fit Hubble constant. These 33 distances imply a Hubble constant of  $H_0 = 60 \text{ km s}^{-1} \text{ Mpc}^{-1}$  for an open  $\Omega_M = 0.3$  universe and  $H_0 = 58 \text{ km s}^{-1} \text{ Mpc}^{-1}$  for a flat  $\Omega_M = 1$  cosmology.

As the quality of SZE and X-ray data improves, it will be possible to employ ICM models more sophisticated than the spherical  $\beta$ -models currently used. Nevertheless, inspection of Fig. 5.1 already provides confidence that a survey of SZE distances consisting of perhaps a few hundred clusters with redshifts extending to one and beyond would allow the technique to be used to trace the expansion history of the universe, providing a valuable independent check of the type Ia supernova results.<sup>31,32</sup>

## 5.2 Gas Masses, Baryonic Mass Fractions, and $\Omega_M$

As outlined in Sec. 3.3, the ratio of the gas mass of a cluster to its total gravitational mass provides a lower limit to its total baryon fraction. After compensating for the baryons contained in the galaxies and those lost during cluster formation, the gas mass fraction should reflect the universal baryon fraction  $\Omega_B/\Omega_M$ . Therefore a determination of the gas mass fraction combined with constraints on  $\Omega_B$  leads to an estimate of  $\Omega_M$ . Here we use  $\Omega_B h_{100}^2 = 0.019 \pm 0.002$  determined from observations of D/H in Ly $\alpha$  clouds<sup>39,40</sup> along with recent reanalysis of big bang nucleosynthesis predictions.<sup>37,38</sup> Such an estimate of  $\Omega_M$  is still strictly an upper bound, as we cannot rule out the possibility of additional reservoirs of baryons in galaxy clusters which have yet to be detected.

Two samples of SZE clusters have been analyzed and the results used to place constraints on  $\Omega_M$ ; a sample of four nearby clusters<sup>70</sup> and a sample of 18 distant clusters.<sup>22,23</sup> Both analyses

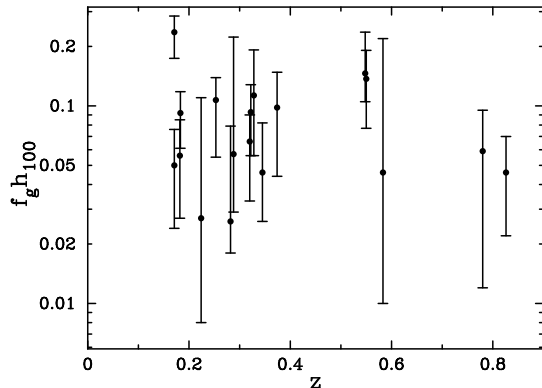


Figure 12: The gas mass fraction scaled to  $r_{500}$  for galaxy clusters derived from OVRO and BIMA Sunyaev-Zel'dovich effect data as a function of redshift assuming a  $\Omega_M = 0.3$ ,  $\Omega_\Lambda = 0.7$  cosmology.<sup>22,23</sup> The mean gas mass fraction is  $f_g = 0.081^{+0.009}_{-0.011} h_{100}^{-1}$ .

used a spherical isothermal  $\beta$ -model for the ICM. The nearby sample was observed with the Owens Valley 5.5 m telescope at 32 GHz as part of a SZE study of an X-ray flux limited sample.<sup>70</sup> In this study, the integrated SZE is used to normalize a model for the gas density from published X-ray analyses, and this gas mass is compared to the published total masses to determine the gas mass fraction within radii of 1-1.5  $h_{100}^{-1}$  Mpc. For three clusters, A2142, A2256 and the Coma cluster, a gas mass fraction of  $(0.061 \pm 0.011)h_{100}^{-1}$  is found; for the cluster Abell 478, a gas mass fraction of  $(0.16 \pm 0.014)h_{100}^{-1}$  is reported.

The high redshift sample of 18 clusters ( $0.14 < z < 0.83$ ) was observed interferometrically at 30 GHz using the OVRO and BIMA SZE imaging system.<sup>22,23</sup> In this study the model for the gas density was determined directly by the SZE data; no X-ray imaging data was used. X-ray derived emission weighted temperatures were used, however. The gas mass fractions were computed from the data at a  $1'$  radius where they are best constrained by the observations. Numerical simulations suggest, however, that the gas mass fraction at  $r_{500}$  (the radius at which the enclosed mean density of the cluster is 500 times the critical density) should reflect the universal baryon fraction.<sup>105,106,43</sup> The derived gas mass fractions were therefore extrapolated to  $r_{500}$  using scaling relations from cluster simulations.<sup>105</sup>

The resulting gas mass fractions assuming a  $\Omega_M = 0.3$ ,  $\Omega_\Lambda = 0.7$  cosmology for each cluster are shown as a function of redshift in Fig. 12. The uncertainty in the electron temperatures contribute the largest component to the error budget. The resulting mean gas mass fractions are  $f_g = 0.081^{+0.009}_{-0.011} h_{100}^{-1}$  for  $\Omega_M = 0.3$ ,  $\Omega_\Lambda = 0.7$ ,  $f_g = 0.074^{+0.008}_{-0.009} h_{100}^{-1}$  for  $\Omega_M = 0.3$ ,  $\Omega_\Lambda = 0.0$  and  $f_g = 0.068^{+0.009}_{-0.008} h_{100}^{-1}$  for  $\Omega_M = 1.0$ ,  $\Omega_\Lambda = 0.0$ .

Gas mass fractions derived from X-ray images for a large, homogeneous, nearby sample of clusters are presented in Mohr et al. (1999).<sup>46</sup> For a subsample of 28 clusters with  $T_e > 5$  keV, they find the mean gas mass fraction within  $r_{500}$  to be  $(0.0749 \pm 0.0021)h_{100}^{-3/2}$  at 90% confidence. The gas mass fractions derived from SZE measurements depend differently on the cosmology assumed than those derived from X-ray images, and this should be noted when comparing the results. Qualitatively, the comparison does not suggest any large systematic offsets. This is significant, because a large clumping factor,  $C \equiv \langle n_e^2 \rangle^{1/2} / \langle n_e \rangle$ , has been suggested as an explanation for the high gas mass fractions in clusters.<sup>35,105</sup> A cluster with clumping factor  $C$  would only require  $1/C$  as much gas mass to produce the observed emission, and the SZE and X-ray gas mass fraction measurements would differ by a factor of  $\sim C$ .

The measured gas mass fractions can be used to determine  $\Omega_M$  in a self-consistent manner. Fig. 13 shows the value of  $\Omega_M$  implied by the measured gas mass fractions assuming a flat universe ( $\Omega_\Lambda \equiv 1 - \Omega_M$ ) and  $h = 0.7$  to calculate the angular diameter distance and  $r_{500}$  scaling

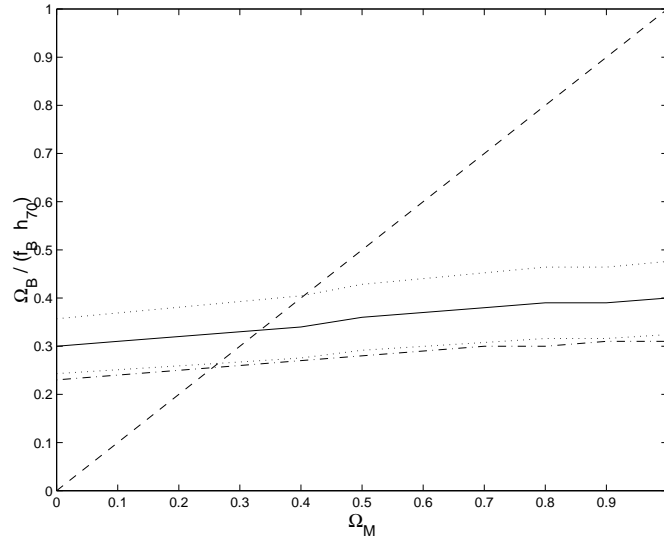


Figure 13: Limits on  $\Omega_M$  from SZE measured cluster gas fractions.<sup>23</sup> Upper limit on the total matter density,  $\Omega_M \leq \Omega_B/(f_B h_{70})$  (full line) and its associated 68% confidence region (dotted lines), as a function of cosmology with  $\Omega_\Lambda \equiv 1 - \Omega_M$ . The intercept between the upper dotted line and the dashed line  $\Omega_M = \Omega_B/(f_B h_{70})$  gives the upper limit to  $\Omega_M$  at 68% confidence. The dot-dashed line shows the total matter density when the baryon fraction includes an estimate of the contribution from baryons in galaxies and those lost during cluster formation. The intercept of the dot-dashed line and the dashed line gives the best estimate of  $\Omega_M \sim 0.25$  assuming a flat universe with  $h = 0.7$ .

factor. The upper limit to  $\Omega_M$  and its associated 68% confidence interval is shown as a function of  $\Omega_M$ . The measured gas mass fractions are consistent with a flat universe and  $h = 0.7$  when  $\Omega_M$  is less than 0.40, at 68% confidence. For the measurements to be consistent with  $\Omega_M = 1.0$  in a flat universe, the Hubble constant must be very low,  $h$  less than  $\sim 0.30$ .

For a more realistic estimate, an attempt is made to account for the baryon contribution from galaxies and those lost during cluster formation. The mass of the cluster galaxies is assumed to be a fixed fraction of the cluster gas mass, with the fraction fixed at the value observed in the Coma cluster,  $M_{gas} = M_g(1 + 0.20h_{100}^{3/2})$ .<sup>35</sup> The gas in the cluster will be more extended than the dark matter and the baryon fraction at  $r_{500}$  will be a modest underestimate of the true baryon fraction  $f_g(r_{500}) = 0.85 \times f_b(\text{universal})$ .<sup>105</sup> These assumptions lead to  $f_B = (f_g(1 + 0.20h_{100}^{3/2})/0.85)$  Using this to scale the gas mass fractions derived from the high  $z$  cluster sample and assuming  $h = 0.7$  and a flat cosmology, leads to the constraints illustrated in Fig. 13. The best estimate of  $\Omega_M$  is  $\sim 0.25$ .

### 5.3 Cluster Peculiar Velocities

The kinetic SZE signal from the peculiar velocity of galaxy clusters is very small ( $\leq 0.1$  mK) and difficult to detect. Disentangling the thermal and kinetic SZE's requires multi-frequency SZE observations. To date there have been only a few recent attempts to measure the effect.

The first interesting limits on the peculiar velocity of a galaxy cluster were reported in Holzapfel et al. (1997).<sup>33</sup> They used SuZIE to observe Abell 2163 ( $z = 0.201$ ) and Abell 1689 ( $z = 0.181$ ) at 140 GHz (2.1 mm), 218 GHz (1.4 mm) and 270 GHz (1.1 mm). These observations include and bracket the null in the thermal SZE spectrum. Using a  $\beta$  model, with the shape parameters  $(\theta_c, \beta)$  from X-ray data, they find  $V_p = +490_{-880}^{+1370}$  km s<sup>-1</sup> for Abell 2163 and

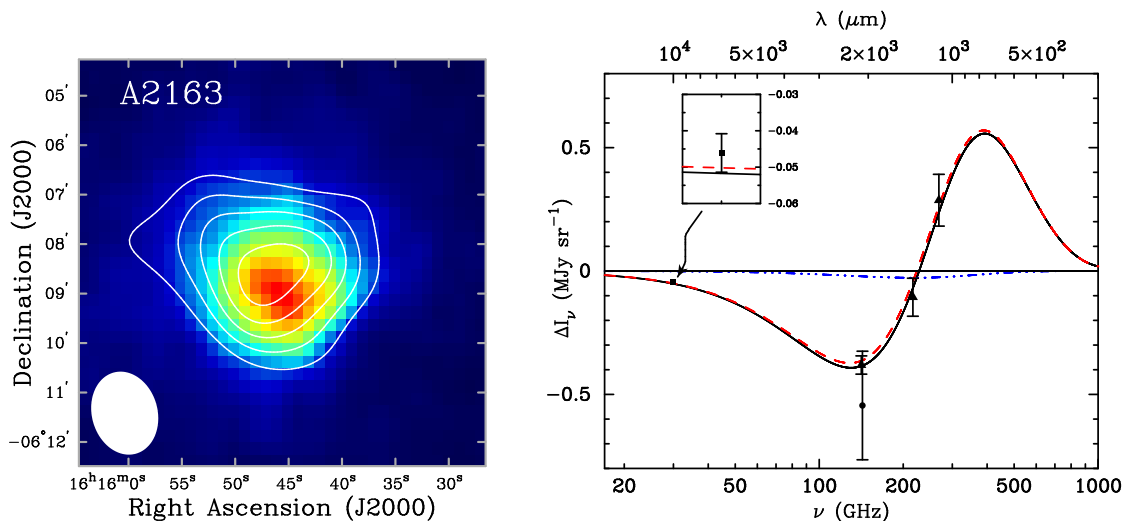


Figure 14: Left panel: An image of the SZE effect toward Abell 2163 obtained with the BIMA interferometer overlaid on a ROSAT image of the X-ray emission. Right panel: the SZE spectrum of Abell 2163 using data from BIMA at 28.5 GHz,<sup>34</sup> DIABOLO at 140 GHz<sup>72</sup> (filled circle) and SuZIE at 140 GHz, 218 GHz and 270 GHz<sup>33</sup> (filled triangles). The best fit thermal and kinetic SZE spectra are shown by the dot-dashed line and the dashed lines, respectively, with the spectra of the combined effect shown by the solid line. The limits on the Compton  $y$ -parameter and the peculiar velocity are  $y_0 = 3.65 \pm 0.40 \times 10^{-4}$  and  $v_p = 415_{-765}^{+920}$  km s<sup>-1</sup>.<sup>33,34</sup>

$V_p = +170_{-630}^{+815}$  km s<sup>-1</sup> for Abell 1689, where the uncertainties are at 68% confidence and include both statistical and systematic uncertainties. These results are limited by the sensitivity of these SZE observations, which are limited by differential atmospheric emission. The SuZIE data for Abell 2163 have been reanalyzed with the addition of higher frequency measurements which are sensitive to emission from Galactic dust in the direction of the cluster.<sup>100</sup> More recently LaRoque et al. (2000)<sup>34</sup> also reanalyzed all of the available data for Abell 2163, including a new measurement obtained with the OVRO and BIMA SZE imaging system at 30 GHz (1 cm). As shown in Fig. 14, they find the data is well fitted by parameters remarkably similar to the original values from Holzapfel et al. with insignificant contamination by Galactic dust emission when the SuZIE observing scheme is taken into account.

## 6 Summary

We have reviewed the large amount of progress made in detecting and imaging the SZE over the last several years. The SZE has lived up to its initial promise of providing an independent estimate of the Hubble constant. It has also been used to estimate the matter density of the universe. The full potential of the SZE as a cosmological tool, however, is largely unrealized; the SZE is ideally suited for conducting large, deep, surveys for clusters. As discussed in Sec. 3.4, SZE surveys are particularly powerful since the cluster detection threshold for such a survey is the cluster mass and is essentially independent of redshift.

SZE surveys will provide a direct view of structure formation in the high-redshift universe; if clusters exist at redshifts much higher than currently predicted they will be found by the SZE survey, but missed in even the deepest X-ray observations planned.

A deep SZE survey can expect to find roughly one cluster per square degree with  $z > 1.5$ . The large sample of high redshift clusters found in such a survey can be followed up with X-

ray observations and then used to refine SZE  $H_o$  estimates and even constrain the deceleration parameter, providing a valuable check of the type Ia supernova results.<sup>31,32</sup>

Most importantly, using the data from SZE surveys to determine the evolution of the number density and mass distribution of clusters will lead to tight constraints on  $\Omega_M$ ,  $\Omega_\Lambda$ , and even the equation of state for the dark energy.<sup>4</sup>

Lastly, surveys with fairly high angular resolution ( $\sim 30''$ ) will be sensitive to the evolution of the intracluster medium,<sup>57</sup> perhaps seeing the effects of feedback from galaxy formation out to  $z \sim 2$ .

While the present instruments and techniques have led to remarkable progress (see Secs. 4.2 and 4.3), they are much too slow to conduct the large, deep, SZE surveys we envision. In some ways, the current instruments are prototypes of the instruments needed to conduct large SZE surveys. Due to the success of these instruments, we now have the knowledge to design powerful SZE survey instruments. Both dedicated interferometric arrays and single dish telescopes equipped with large bolometric arrays are likely to conduct deep surveys over tens of square degrees in the near future.

SZE survey machines that are currently being built or awaiting funding include interferometric arrays (SZA by the OVRO – BIMA SZE imaging group, AMI by the Ryle SZE imaging group, AMiBA in Taiwan, and upgrades to CBI and DASI) and bolometric arrays (ACBAR on the Viper telescope at the South pole, BOLOCAM on the CSO telescope on Mauna Kea, and a large format bolometer array on a  $\sim 10\text{m}$  telescope located at the South Pole (SPST)). All of these instruments will be capable of surveying tens of square degrees, if not much more, per year. The interferometers are likely to provide the highest resolution and deepest images, while the bolometric arrays are likely to provide the largest sky coverage. Both will be needed to fully exploit the power of the SZE as a cosmological tool.

## Acknowledgment

This work is supported in part by NASA LTSA grant NAG5-7986. We thank Mike Joffre, Amber Miller, and Daisuke Nagai for helpful comments and discussions. JEC acknowledges generous support from the David and Lucile Packard Foundation and the James S. McDonnell Foundation. We thank the conference organizers for an enjoyable and stimulating conference.

## References

1. R.A. Sunyaev and Y.B. Zel'dovich. The spectrum of primordial radiation, its distortions and their significance. *Comments Astrophys. Space Phys.*, 2:66, 1970.
2. R.A. Sunyaev and Y.B. Zel'dovich. The observation of relic radiation as a test of the nature of x-ray radiation from the clusters of galaxies. *Comments Astrophys. Space Phys.*, 4:173, 1972.
3. G. P. Holder, J. J. Mohr, J. E. Carlstrom, Evrard A. E., and E. M Leitch. Expectations for an interferometric Sunyaev-Zel'dovich effect survey for galaxy clusters. *ApJ*, 544:629, 2000.
4. Z. Haiman, J. J. Mohr, and G. P. Holder. Constraints on cosmological parameters from future galaxy cluster surveys. *ApJ*, submitted: astro-ph/0002336, 2000.
5. D. J. Fixsen, E. S. Cheng, J. M. Gales, J. C. Mather, R. A. Shafer, and E. L. Wright. The cosmic microwave background spectrum from the full COBE FIRAS data set. *ApJ*, 473:576, December 1996.
6. R.A. Sunyaev and Y.B. Zel'dovich. Microwave background radiation as a probe of the contemporary structure and history of the universe. *ARAA*, 18:537, 1980.

7. Y. Rephaeli. Comptonization of the cosmic microwave background: The Sunyaev-Zel'dovich effect. *Ann. Rev. Astron. Astrophys.*, 33:541, 1995.
8. M. Birkinshaw. The Sunyaev-Zel'dovich effect. *Physics Reports*, 310:97, 1999.
9. Y. Rephaeli and D. Yankovitch. Relativistic corrections in the determination of  $H_0$  from x-ray and Sunyaev-Zel'dovich measurements. *ApJ*, 481:L55, June 1997.
10. N. Itoh, Y. Kohyama, and S. Nozawa. Relativistic corrections to the Sunyaev-Zel'dovich effect for clusters of galaxies. *ApJ*, 502:7, July 1998.
11. A. Challinor and A. Lasenby. Relativistic corrections to the Sunyaev-Zel'dovich effect. *ApJ*, 499:1, May 1998.
12. S. Nozawa, N. Itoh, and Y. Kohyama. Relativistic corrections to the Sunyaev-Zel'dovich effect for clusters of galaxies. II. inclusion of peculiar velocities. *ApJ*, 508:17, November 1998.
13. S. Y. Sazonov and R. A. Sunyaev. Cosmic microwave background radiation in the direction of a moving cluster of galaxies with hot gas: Relativistic corrections. *ApJ*, 508:1, November 1998.
14. P. R. Phillips. Calculation of the kinetic Sunyaev-Zel'dovich effect from the Boltzmann equation. *ApJ*, 455:419, December 1995.
15. R. F. Mushotzky and C. A. Scharf. The luminosity-temperature relation at  $z = 0.4$  for clusters of galaxies. *ApJ*, 482:L13, June 1997.
16. S. W. Allen and A. C. Fabian. The impact of cooling flows on the  $t_x-l_{Bol}$  relation for the most luminous clusters. *M.N.R.A.S.*, 297:L57, July 1998.
17. J. Miralda-Escude and A. Babul. Gravitational lensing in clusters of galaxies: New clues regarding the dynamics of intracluster gas. *ApJ*, 449:18, August 1995.
18. A. Loeb and S. Mao. Evidence from gravitational lensing for a nonthermal pressure support in the cluster of galaxies Abell 2218. *ApJ*, 435:L109, November 1994.
19. X. Wu and L. Fang. A statistical comparison of cluster mass estimates from optical/x-ray observations and gravitational lensing. *ApJ*, 483:62, July 1997.
20. G. Squires and N. Kaiser. Unbiased cluster lens reconstruction. *ApJ*, 473:65, December 1996.
21. M. Joy, S. Laroque, L. Grego, Carlstrom J. E., K. Dawson, H. Ebeling, W. L. Holzzapfel, D. Nagai, and E. D. Reese. Sunyaev-Zel'dovich effect imaging of massive clusters of galaxies at redshift  $> 0.8$ . *ApJ*—submitted, 2000.
22. L. Grego. *Galaxy Cluster Gas Fractions from Interferometric Measurements of the Sunyaev-Zel'dovich Effect*. PhD thesis, Caltech, 1999.
23. L. Grego, J. E. Carlstrom, E.D. Reese, G. P. Holder, W.L. Holzzapfel, M. Joy, J.J. Mohr and S. Patel Galaxy Cluster Gas Mass Fractions from Sunyaev-Zel'dovich Effect Measurements: Constraints on  $\Omega_M$  *ApJ*, in press, 2001.
24. A. Cavaliere, L. Danese, and G. de Zotti. Unborn clusters. *ApJ*, 217:6, October 1977.
25. J. E. Gunn. The Friedmann models and optical observations in cosmology. In *Observational Cosmology Advanced Course*, page 1, 1978.
26. J. Silk and S. D. M. White. The determination of  $q_0$  using x-ray and microwave observations of galaxy clusters. *ApJ*, 226:L103, December 1978.
27. A. Cavaliere and R. Fusco-Femiano. The distribution of hot gas in clusters of galaxies. *Astron. Astrophys.*, 70:677, 1978.
28. P. E Boynton and S. S. Murray. *HEAO B Guest Observer proposal*, 1978.
29. M. Birkinshaw. Limits to the value of the Hubble constant deduced from observations of clusters of galaxies. *M.N.R.A.S.*, 187:847, June 1979.
30. M. E. Sulkanen. Galaxy cluster shapes and systematic errors in  $H_0$  measured by the Sunyaev-Zel'dovich effect. *ApJ*, 522:59, September 1999.
31. A. G. Riess, A. V. Filippenko, P. Challis, A. Clocchiattia, A. Diercks, P. M. Garnavich,

- R. L. Gilliland, C. J. Hogan, S. Jha, R. P. Kirshner, B. Leibundgut, M. M. Phillips, D. Reiss, B. P. Schmidt, R. A. Schommer, R. C. Smith, J. Spyromilio, C. Stubbs, N. B. Suntzeff, and J. Tonry. Observational evidence from supernovae for an accelerating universe and a cosmological constant. *A.J.*, 116:1009, 1998.
32. S. Perlmutter, G. Aldering, G. Goldhaber, R.A. Knop, P. Nugent, P.G. Castro, S. Deustua, S. Fabbro, A. Goobar, D. E. Groom, I. M. Hook, A. G. Kim, M.Y. Kim, J.C. Lee, N.J. Nunes, R. Pain, C.R. Pennypacker, R. Quimby, C. Lidman, R.S. Ellis, M. Irwin, R.G. McMahon, P. Ruiz-Lapuente, N. Walton, B. Schaefer, B.J. Boyle, A.V. Filippenko, T. Matheson, A.S. Fruchter, N. Panagia, H. J .M. Newberg, and W.J. Couch. Measurements of  $\Omega$  and  $\Lambda$  from 42 high-redshift supernovae. *ApJ*, 517:565, 1999.
  33. W. L. Holzappel, P. A. R. Ade, S. E. Church, P. D. Mauskopf, Y. Rephaeli, T. M. Wilbanks, and A. E. Lange. Limits on the peculiar velocities of two distant clusters using the kinematic Sunyaev-Zel'dovich effect. *ApJ*, 481:35, May 1997.
  34. S. J. LaRoque, E. D. Reese, J. E. Carlstrom, W. L. Holzappel, M. Joy, and L. Grego. The Sunyaev-Zel'dovich effect spectrum in Abell 2163. *ApJ*, submitted, 2000.
  35. S.D.M. White, J.F. Navarro, A.E. Evrard, and C.S. Frenk. The baryon content of galaxy clusters: A challenge to cosmological orthodoxy. *Nature*, 366:429, 1993.
  36. W. Forman and C. Jones. X-ray-imaging observations of clusters of galaxies. *Ann. Rev. Astron. Astrophys.*, 20:547, 1982.
  37. K. M. Nollett and S. Burles. Estimating reaction rates and uncertainties for primordial nucleosynthesis. *Phys. Rev. D*, 61:123505, 2000.
  38. S. Burles, K.M. Nollett, J.N Truran, and M.S Turner. Sharpening the predictions of big-bang nucleosynthesis. *Phys. Rev. Lett.*, 82:4176, 1999.
  39. S. Burles and D. Tytler. The deuterium abundance toward QSO 1009+2956. *ApJ*, 507:732, 1998.
  40. S. Burles and D. Tytler. The deuterium abundance toward QSO 1937-1009. *ApJ*, 499:699, 1998.
  41. G. P. Holder, J. E. Carlstrom, and A. E. Evrard. Combining interferometric Sunyaev-Zel'dovich effect measurements and weak lensing. In F. Durret and G. Gerbal, editors, *Constructing the Universe with Clusters of Galaxies*, IAP, 2000.
  42. D. A. White and A. C. Fabian. Einstein observatory evidence for the widespread baryon overdensity in clusters of galaxies. *M.N.R.A.S.*, 273:72, March 1995.
  43. L.P. David, C. Jones, and W. Forman. Cosmological implications of ROSAT observations of groups and clusters of galaxies. *ApJ*, 445:578, 1995.
  44. D. M. Neumann and H. Bohringer. X-ray properties of the distant cluster CL 0016+16. *M.N.R.A.S.*, 289:123, July 1997.
  45. G. Squires, D. M. Neumann, N. Kaiser, M. Arnaud, A. Babul, H. Boehringer, G. Fahlman, and D. Woods. Weak gravitational lensing and x-ray analysis of Abell 2163. *ApJ*, 482:648, June 1997.
  46. J.J. Mohr, B. Mathiesen, and A.E. Evrard. Properties of the intracluster medium in an ensemble of nearby galaxy clusters. *ApJ*, 517:627, 1999.
  47. P.T.P. Viana and A.R. Liddle. Galaxy clusters at  $0.3 < z < 0.4$  and the value of  $\Omega_0$ . *M.N.R.A.S.*, 303:535, 1999.
  48. N.A. Bahcall and X. Fan. The most massive distant clusters: Determining  $\Omega$  and  $\sigma_8$ . *ApJ*, 504:1, 1998.
  49. J. Oukbir, J. G. Bartlett, and A. Blanchard. X-ray galaxy clusters: Constraints on models of galaxy formation. *Astron. Astrophys.*, 320:365, April 1997.
  50. J. G. Bartlett and J. Silk. The Sunyaev-Zel'dovich effect and cluster evolution. *ApJ*, 423:12, March 1994.
  51. D. Barbosa, J.G. Bartlett, A. Blanchard, and J. Oukbir. The Sunyaev-Zel'dovich effect



- and the value of  $\Omega_0$ . *Astron. Astrophys.*, 314:13, 1996.
52. K. Romer, P. T. P. Viana, A. R. Liddle, and R. G. Mann. A serendipitous galaxy cluster survey with XMM. In *Large Scale Structure in the X-ray Universe, Proceedings of the 20-22 September 1999 Workshop, Santorini, Greece, eds. Plionis, M. & Georgantopoulos, I., Atlantisciences, Paris, France, p.409*, page 409, March 2000.
  53. A. D. Miller, R. Caldwell, M. J. Devlin, W. B. Dorwart, T. Herbig, M. R. Nolta, L. A. Page, J. Puchalla, E. Torbet, and H. T. Tran. A measurement of the angular power spectrum of the cosmic microwave background from  $\ell = 100$  to 400. *ApJ*, 524:L1, October 1999.
  54. P. de Bernardis, P. A. R. Ade, J. J. Bock, J. R. Bond, J. Borrill, A. Boscaleri, K. Coble, B. P. Crill, G. De Gasperis, P. C. Farese, P. G. Ferreira, K. Ganga, M. Giacometti, E. Hivon, V. V. Hristov, A. Iacoangeli, A. H. Jaffe, A. E. Lange, L. Martinis, S. Masi, P. V. Mason, P. D. Mauskopf, A. Melchiorri, L. Miglio, T. Montroy, C. B. Netterfield, E. Pascale, F. Piacentini, D. Pogosyan, S. Prunet, S. Rao, G. Romeo, J. E. Ruhl, F. Scaramuzzi, D. Sforna, and N. Vittorio. A flat universe from high-resolution maps of the cosmic microwave background radiation. *Nature*, 404:955, 2000.
  55. S. Hanany, P. Ade, A. Balbi, J. Bock, J. Borrill, A. Boscaleri, P. de Bernardis, P. G. Ferreira, V. V. Hristov, A. H. Jaffe, A. E. Lange, A. T. Lee, P. D. Mauskopf, C. B. Netterfield, S. Oh, E. Pascale, B. Rabbii, P. L. Richards, G. F. Smoot, R. Stompor, C. D. Winant, and J. H. P. Wu. MAXIMA-1: A measurement of the cosmic microwave background anisotropy on angular scales of 10 arcminutes to 5 degrees. *ApJ*, in press, 2000. astro-ph/0005123.
  56. J. E. Carlstrom, M. K. Joy, L. Grego, G. P. Holder, W. L. Holzapfel, J. J. Mohr, S. Patel, and E. D. Reese. Imaging the Sunyaev-Zel'dovich effect. *Physical Scripta*, vol 60, in press (astro-ph/9905255), 1999.
  57. G. P. Holder and J. E. Carlstrom. Understanding cluster gas evolution with deep Sunyaev-Zel'dovich effect surveys. *ApJ*, in prep., 2001.
  58. M. Birkinshaw. Measurement of the Sunyaev-Zel'dovich effect. In *Physical Cosmology, eds. A. Blanchard, L. Celnikier, M. Lachi'eze-Rey, J. Tran Thanh Van, Editions Frontieres, Gif sur Yvette, France, p. 177*, page 177, 1991.
  59. T. Herbig, C. R. Lawrence, A. C. S. Readhead, and S. Gulkis. A measurement of the Sunyaev-Zel'dovich effect in the Coma cluster of galaxies. *ApJ*, 449:L5, 1995.
  60. G.P. Holder and J.E. Carlstrom. The Sunyaev-Zel'dovich effect as microwave foreground and probe of cosmology. In A. de Oliveira-Costa and M. Tegmark, editors, *Microwave Foregrounds*, San Francisco, 1999. ASP- astro-ph/9904220.
  61. W. L. Holzapfel, J. E. Carlstrom, L. Grego, G. Holder, M. Joy, and E. D. Reese. Limits on arcminute-scale cosmic microwave background anisotropy at 28.5 GHz. *ApJ*, 539:57, August 2000.
  62. K. S. Dawson, W. L. Holzapfel, J. E. Carlstrom, M. Joy, S. J. LaRoque, and E. D. Reese. A preliminary detection of arcminute scale cosmic microwave background anisotropy with the BIMA array. *ApJ*, - submitted: astro-ph/0012151, 2000.
  63. A. R. Cooray, L. Grego, W. L. Holzapfel, M. Joy, and J. E. Carlstrom. Radio sources in galaxy clusters at 28.5 GHz. *A.J.*, 115:1388, April 1998.
  64. A. Loeb and A. Refregier. Effect of gravitational lensing on measurements of the Sunyaev-Zel'dovich effect. *ApJ*, 476:L59, February 1997.
  65. I. Smail, R. J. Ivison, and A. W. Blain. A deep sub-millimeter survey of lensing clusters: A new window on galaxy formation and evolution. *ApJ*, 490:L5, November 1997.
  66. J. P. Hughes and M. Birkinshaw. Another x-ray-discovered poor cluster of galaxies associated with CL 0016+16. *ApJ*, 497:645, 1998.
  67. M. Birkinshaw, S. F. Gull, and K. J. E. Northover. Extent of hot intergalactic gas in the cluster Abell 2218. *Nature*, 275:40, September 1978.

68. M. Birkinshaw, S. F. Gull, and K. J. E. Northover. Measurements of the gas contents of clusters of galaxies by observations of the background radiation at 10.6 GHz. *M.N.R.A.S.*, 185:245, October 1978.
69. M. Birkinshaw. New results on the Sunyaev-Zel'dovich effect in CL 0016+16, Abell 665 and Abell 2218. In *Radio Continuum Processes in Clusters of Galaxies*, page 261, 1986.
70. S. T. Myers, J. E. Baker, A. C. S. Readhead, E. M. Leitch, and T. Herbig. Measurements of the Sunyaev-Zel'dovich effect in the nearby clusters Abell 478, Abell 2142, and Abell 2256. *ApJ*, 485:1, 1997.
71. B. S. Mason, E. M. Leitch, S. T. Myers, J. K. Cartwright and A. C. S. Readhead. An absolute flux density measurement of the supernova remnant cassiopeia A at 32 GHz. *A.J.*, 118:2908, 1999.
72. F. . Desert, A. Benoit, S. Gaertner, J. . Bernard, N. Coron, J. Delabrouille, P. de Marcillac, M. Giard, J. . Lamarre, B. Lefloch, J. . Puget, and A. Sirbi. Observations of the Sunyaev-Zel'dovich effect at high angular resolution towards the galaxy clusters Abell 665, Abell 2163 and CL 0016+16. *New Astronomy*, 3:655, November 1998.
73. P. Andreani, L. Pizzo, G. dall'Oglio, N. Whyborn, H. Boehringer, P. Shaver, R. Lemke, A. Otarola, L. A. Nyman, and R. Booth. Looking for the Sunyaev-Zel'dovich effect toward distant ROSAT clusters of galaxies. *ApJ*, 459:L49, March 1996.
74. W. L. Holzapfel, T. M. Wilbanks, P.A.R. Ade, S. E. Church, M.L. Fischer, P.D. Mauskopf, and A. E. Lange. The Sunyaev-Zel'dovich infrared experiment: A millimeter-wave receiver for cluster cosmology. *ApJ*, 479:17, 1997.
75. P. D. Mauskopf, P. A. R. Ade, S. W. Allen, S. E. Church, A. C. Edge, K. M. Ganga, W. L. Holzapfel, A. E. Lange, B. K. Rownd, B. J. Philhour, and M. C. Runyan. A determination of the Hubble constant using measurements of x-ray emission and the Sunyaev-Zel'dovich effect at millimeter wavelengths in the cluster Abell 1835. *ApJ*, 538:505, August 2000.
76. W. L. Holzapfel, M. Arnaud, P. A. R. Ade, S. E. Church, M. L. Fischer, P. D. Mauskopf, Y. Rephaeli, T. M. Wilbanks, , and Lange A. E. Measurement of the Hubble constant from x-ray and 2.1 millimeter observations of Abell 2163. *ApJ*, 480:449, astro-ph 9702224, 1997.
77. P. Andreani, H. Böhringer, G. Dall'Oglio, L. Martinis, P. Shaver, R. Lemke, L. Å. Nyman, R. Booth, L. Pizzo, N. Whyborn, Y. Tanaka, and H. Liang. The enhancement and decrement of the Sunyaev-Zel'dovich effect toward the ROSAT cluster RX J0658-5557. *ApJ*, 513:23, March 1999.
78. P. D. Mauskopf, B. K. Rownd, S. F. Edgington, V. V. Hristov, A. K. Mainzer, J. Glenn, A. E. Lange, J. J. Bock, and P. A. R. Ade. BOLOCAM: A 144 element bolometer array camera for millimeter-wave imaging. In *Imaging at Radio through Submillimeter Wavelengths. Edited by Jeff Mangum. Publisher: The Astronomical Society of the Pacific, Conference Series, 2000. The conference was held June 6-8, 1999, in Tucson, Arizona.*, page E46, 2000.
79. J. Glenn, J. J. Bock, G. Chattopadhyay, S. F. Edgington, A. E. Lange, J. Zmuidzinas, P. D. Mauskopf, B. Rownd, L. Yuen, and P. A. Ade. BOLOCAM: A millimeter-wave bolometric camera. *Proc. SPIE*, 3357:326, July 1998.
80. M. Jones, R. Saunders, P. Alexander, M. Birkinshaw, N. Dilon, K. Grainge, S. Hancock, A. Lasenby, D. Lefebvre, and G. Pooley. An image of the Sunyaev-Zel'dovich effect. *Nature*, 365:320, September 1993.
81. K. Grainge, M. Jones, G. Pooley, R. Saunders, and A. Edge. Detection of the Sunyaev-Zel'dovich effect in Abell 773. *M.N.R.A.S.*, 265:L57, 1993.
82. J. E. Carlstrom, M. Joy, and L. E. Grego. Interferometric imaging of the Sunyaev-Zel'dovich effect at 30 GHz. *ApJ*, 456:L75, 1996.
83. K. Grainge, M. Jones, G. Pooley, R. Saunders, J. Baker, T. Haynes, and A. Edge. A

- resolved image of the Sunyaev-Zel'dovich effect in Abell 1413. *M.N.R.A.S.*, 278:L17, January 1996.
84. J. E. Carlstrom, L. Grego, W. L. Holzapfel, and M. Joy. Sunyaev-Zel'dovich observations with the OVRO and BIMA arrays. *Eighteenth Texas Symposium on Relativistic Astrophysics and Cosmology*, ed A. Olinto, J. Frieman, and D. Schramm, World Scientific, page 261, 1998.
  85. S. K. Patel, M. Joy, J. E. Carlstrom, G. P. Holder, E. D. Reese, P. L. Gomez, J. P. Hughes, L. Grego, and W. L. Holzapfel. The distance and mass of the galaxy cluster Abell 1995 derived from Sunyaev-Zel'dovich effect and x-ray measurements. *ApJ*–submitted, 2000.
  86. L. Grego, J. E. Carlstrom, M. K. Joy, E. D. Reese, G. P. Holder, S. Patel, A. R. Cooray, and W. L. Holzapfel. The Sunyaev-Zel'dovich effect in Abell 370. *ApJ*, 539:39, August 2000.
  87. E. D. Reese, J. J. Mohr, J. E. Carlstrom, M. Joy, L. Grego, G. P. Holder, W. L. Holzapfel, J. P. Hughes, S. K. Patel, and M. Donahue. Sunyaev-Zel'dovich effect-derived distances to the high-redshift clusters MS 0451.6-0305 and CL 0016+16. *ApJ*, 533:38, April 2000.
  88. M. Jones. *private communication*, 2000.
  89. M. W. Pospieszalski, W. J. Lakatosh, L. D. Nguyen, M. Lui, T. Liu, M. Le, M. A. Thompson, and M. J. Delaney. Q- and E-band cryogenically-coolable amplifiers using AlInAs/GaInAs/InP HEMT's. *IEEE MTT-S Int. Microwave Symp.*, page 1121, 1995.
  90. K. Grainge, M. E. Jones, G. Pooley, R. Saunders, A. Edge, and R. Kneissl. Measuring the Hubble constant from Ryle telescope and x-ray observations, with application to Abell 1413. *M.N.R.A.S.*–submitted: astro-ph/9904165, 2000.
  91. E. Komatsu, T. Kitayama, Y. Suto, M. Hattori, R. Kawabe, H. Matsuo, S. Schindler, and K. Yoshikawa. Submillimeter detection of the Sunyaev-Zel'dovich effect toward the most luminous x-ray cluster at  $z = 0.45$ . *ApJ*, 516:L1, May 1999.
  92. E. Komatsu, H. Matsuo, T. Kitayama, M. Hattori, R. Kawabe, K. Kohno, N. Kuno, and Y. Suto. Substructures revealed by the Sunyaev-Zel'dovich effect at 150 GHz in the high resolution map of RXJ1347-1145. *PASJ* – *submitted: astro-ph/0006293*, 2000.
  93. E. Pointecouteau, M. Giard, A. Benoit, F. X. Désert, N. Aghanim, N. Coron, J. M. Lamarre, and J. Delabrouille. A Sunyaev-Zel'dovich map of the massive core in the luminous x-ray cluster RX J1347-1145. *ApJ*, 519:L115, July 1999.
  94. E. Pointecouteau, M. Giard, F. X. Désert, B. Alain, J. P. Bernard, J. M. Lamarre, and N. Coron. Extended SZ map of the most luminous x-ray cluster, RXJ1347-1145. *ApJ*, in press: astro-ph/0012309, 2001.
  95. P. S. Udomprasert, B. S. Mason, and A. C. S. Readhead. The Sunyaev-Zel'dovich effect with the cosmic background imager. In F. Durret and G. Gerbal, editors, *Constructing the Universe with Clusters of Galaxies*, IAP, 2000.
  96. S. Padin, J. K. Cartwright, B. S. Mason, A. C. S. Readhead, M. C. Shepherd, J. Sievers, P. S. Udomprasert, W. L. Holzapfel, S. T. Myers, J. E. Carlstrom, E. M. Leitch, M. Joy, L. Bronfman, and J. May. First intrinsic anisotropy observations with the cosmic background imager. *ApJ*, submitted: astro-ph/0012211, 2000.
  97. E. D. Reese, J. E. Carlstrom, J. J. Mohr, M. Joy, L. Grego, and W. L. Holzapfel. A determination of the Hubble constant based on Sunyaev-Zel'dovich effect derived distances to a large sample of high redshift galaxy clusters. *ApJ*, in prep., 2000.
  98. R. Saunders, R. Kneissl, K. Grainge, M. E. Jones, A. Maggi, R. Das, A. Edge, A. N. Lasenby, G. Pooley, S. J. Miyoshi, T. Tsuruta, K. Yamashita, Y. Tawara, A. Furuzawa, A. Harada, and I. Hatsukade. A measurement of  $H_0$  from Ryle telescope, ASCA and ROSAT observations of Abell 773. *M.N.R.A.S.*–submitted: astro-ph/9904168, 2000.
  99. B. S. Mason. *An Improved Measurement of the Hubble Constant Using the Sunyaev-Zel'dovich Effect*. PhD thesis, University of Pennsylvania, 1999.

100. J. M. Lamarre, M. Giard, E. Pointecouteau, J. P. Bernard, G. Serra, F. Pajot, F. X. Desert, I. Ristorcelli, J. P. Torre, S. Church, N. Coron, J. L. Puget, and J. J. Bock. First measurement of the submillimeter Sunyaev-Zel'dovich effect. *ApJ*, 507:L5, 1998.
101. M. Tsuboi, A. Miyazaki, T. Kasuga, H. Matsuo, and N. Kuno. Measurement of the Sunyaev-Zel'dovich effect toward Abell 2218 at 36 GHz. *Proc. Astron. Soc. Japan*, 50:169, February 1998.
102. J. P. Hughes and M. Birkinshaw. A measurement of the Hubble constant from the x-ray properties and the Sunyaev-Zel'dovich effect of CL 0016+16. *ApJ*, 501:1, July 1998.
103. M. Birkinshaw and J. P. Hughes. A measurement of the Hubble constant from the x-ray properties and the Sunyaev-Zel'dovich effect of Abell 2218. *ApJ*, 420:33, January 1994.
104. E. D. Reese, J. E. Carlstrom, J. J. Mohr, M. Joy, L. Grego, and W. L. Holzapfel. Sunyaev-Zel'dovich determined distances to high redshift galaxy clusters. In F. Durret and G. Gerbal, editors, *Constructing the Universe with Clusters of Galaxies*, IAP, 2000.
105. A.E. Evrard. The intracluster gas fraction in x-ray clusters: Constraints on the clustered mass density. *M.N.R.A.S.*, 292:289, 1997.
106. A. E. Evrard, C. A. Metzler, and J. F. Navarro. Mass estimates of x-ray clusters. *ApJ*, 469:494, October 1996.